NeuroImage 90 (2014) 163–178

Contents lists available at ScienceDirect

NeuroImage

journal homepage: www.elsevier.com/locate/ynimg

Plausibility Tracking: A method to evaluate anatomical connectivity and microstructural properties along fiber pathways ☆

Jan Schreiber [a,*], Till Riffert [a], Alfred Anwander [b], Thomas R. Knösche [a]

[a] Max Planck Institute for Human Cognitive and Brain Sciences, Cortical Networks and Cognitive Functions, Leipzig, Germany
[b] Max Planck Institute for Human Cognitive and Brain Sciences, Department of Neuropsychology, Leipzig, Germany

ARTICLE INFO

Article history:
Accepted 1 January 2014
Available online 11 January 2014

Keywords:
Diffusion MRI
Tract-based analysis
Tractography
Global tractography
Spherical deconvolution
Microstructural metrics
Fiber density

ABSTRACT

Diffusion MRI is a non-invasive method that potentially gives insight into the brain's white matter structure regarding the pathway of connections and properties of the axons.
Here, we propose a novel global tractography method named Plausibility Tracking that provides the most plausible pathway, modeled as a smooth spline curve, between two locations in the brain. Compared to other tractography methods, plausibility tracking combines the more complete connectivity pattern of probabilistic tractography with smooth tracks that are globally optimized using the fiber orientation density function and hence is relatively robust against local noise and error propagation. It has been tested on phantom and biological data and compared to other methods of tractography. Plausibility tracking provides reliable local directions all along the fiber pathways which makes it especially interesting for tract-based analysis in combination with direction dependent indices of diffusion MRI.
In order to demonstrate this potential of plausibility tracking, we propose a framework for the assessment and comparison of diffusion derived tissue properties. This framework comprises atlas-guided parameterization of tract representation and advanced bundle-specific indices describing fiber density, fiber spread and white matter complexity. We explore the new method using real data and show that it allows for a more specific interpretation of the white matter's microstructure compared to rotationally invariant indices derived from the diffusion tensor.

Introduction

Diffusion weighted magnetic resonance imaging (dMRI) is a non-invasive technique to evaluate microstructural properties of the brain. It is based on MRI sequences that measure the direction dependent diffusion of water molecules within biological tissue. Structures like cell membranes, myelin sheaths and filaments act as barriers that hinder or restrict this movement and lead to anisotropic diffusion profiles (Beaulieu, 2002). Depending on the type of tissue and the employed imaging protocol, the dMRI measurements are sensitive to particular aspects of the *diffusion propagator*, which gives the probability of a particle diffusing from one point to another within a certain time (for a detailed explanation refer, e.g., to Jones et al., 2013). Different local models for the diffusion propagator have been introduced, ranging from the simple diffusion tensor (Basser et al., 1994) to more sophisticated expressions that, to a certain extent, differentiate between the diffusion of different fiber bundles within one voxel (Aganj et al., 2010; Assaf et al., 2004; Behrens et al., 2007; Schultz and Seidel, 2008; Tuch, 2004; Wedeen et al., 2000; for a review see Alexander, 2005). Alternatively, explicit models of microstructural properties can be used, such as the *fiber orientation density function* (fODF) computed by *spherical deconvolution* (SD) (Dell'Acqua et al., 2007; Descoteaux et al., 2009; Kaden et al., 2008; Tournier et al., 2004, 2007) or various models for the axonal diameter distribution (Assaf et al., 2008; Zhang et al., 2011a,b).

For the most part, dMRI is used to characterize long-range white matter fiber tracts that connect cortical and subcortical gray matter areas. There are two principal approaches. First, one may map voxel-based indices derived from the local (i.e., voxel-wise) dMRI signal (Jones et al., 2005), which are sensitive to some aspects of the microstructural properties and spatial arrangement of nerve fibers as well as other white matter elements (e.g., oligodendrocytes). The by far most commonly used such index is the *fractional anisotropy* (FA)

Abbreviations: MRI, magnetic resonance imaging; dMRI, diffusion magnetic resonance imaging; fODF, fiber orientation density function; FA, fractional anisotropy; MD, mean diffusivity; AD, axial diffusivity; RD, radial diffusivity; SD, spherical deconvolution; CSD, constrained spherical deconvolution; CHARMED, composite hindered and restricted model of diffusion; HARDI, high angular resolution diffusion imaging; FD, fiber density; AFD, angular fiber density; AFD_{max}, maximal angular fiber density; FS, fiber spread; GRAPPA, generalized auto calibrating partially parallel acquisitions; CC, corpus callosum; PFC, prefrontal cortex; BA45, Brodmann area 45; MC, motor cortex; ILF, inferior longitudinal fasciculus; SLF, superior longitudinal fasciculus; CR, corona radiate; IFOF, inferior fronto-occipital fasciculus; ROI, region of interest; MAD, median absolute deviation; MNI, Montreal Neurological Institute.

* Corresponding author at: Max Planck Institute for Human Cognitive and Brain Sciences, Stephanstrasse 1A, 04103 Leipzig, Germany. Fax: +49 341 9940 2260.
E-mail address: schreiber@cbs.mpg.de (J. Schreiber).

1053-8119/$ – see front matter © 2014 The Authors. Published by Elsevier Inc. All rights reserved.
http://dx.doi.org/10.1016/j.neuroimage.2014.01.002

introduced by Basser and Pierpaoli (1996). Standard mapping methods include *voxel-based analysis* (VBA) (Ashburner and Friston, 2000) and *region* or *atlas-based analysis* (Faria et al., 2010; Snook et al., 2007). Second, diffusion tractography (Mori and van Zijl, 2002) interprets the local diffusion signal in terms of fiber directions and then integrates this information over voxels, thereby generating fiber pathways between different brain regions. Major types of tractography algorithms include *deterministic tractography* that always follows the most probable fiber direction (Descoteaux et al., 2009; Lazar et al., 2003; Malcolm et al., 2009; Mori and van Zijl, 2002; Tournier et al., 2012; for a review, see, Lenglet et al., 2009), *probabilistic tractography* estimating a distribution of possible pathways (Anwander et al., 2007; Behrens et al., 2003; Jeurissen et al., 2011; Kaden et al., 2007; Koch et al., 2002) and various *global tractography* methods (Jbabdi et al., 2007; Kreher et al., 2008).

While mapping of indices readily provides an overview on microstructural properties of the tissue (as far as the dMRI signal does provide this information – for a critical review, see Jones et al., 2013) – any assignment to connections between particular brain regions remains rather vague. Tractography, on the other hand, yields specific information on the existence and the course of fiber connections (again, within certain limits, see Jones et al., 2013), without yielding straightforward information on tissue properties other than fiber direction.

It is fairly obvious to look for combinations of both methods, that is, to map indices onto reconstructed fiber pathways, in order to achieve the best possible characterization of a connection. Such *tract-based analysis* (TBA) techniques have been proposed before and range from simple averaging of the FA over the fiber tract volume (Lebel et al., 2008) to more sophisticated parameterization along the tracts (e.g., Corouge et al., 2006).

However, there are several potential shortcomings in such algorithms. First, most of today's methods focus on rotationally invariant indices derived from the diffusion tensor (Basser et al., 1994), as they are fairly sensitive to changes and differences in tissue properties and relatively easy to handle. The downside of these and similar indices is that they are rather unspecific with respect to their possible underlying microstructural traits and that they disregard part of the information contained in modern *high angular resolution diffusion imaging* (HARDI) (Frank, 2002; Tuch, 2002). While there are a number of sophisticated approaches aiming at the estimation of specific microstructural traits, such as axonal density and axonal caliber, from dMRI (Alexander et al., 2010; Assaf et al., 2004, 2008; Zhang et al., 2011a,b), these usually require non-standard acquisition schemes that might not always fit into the routine of neuroscientific research and clinical practice. Recently, however, there have been some attempts to define more informative indices even on the basis of standard HARDI data (Dell'Acqua et al., 2013; Riffert et al., 2012; Savadjiev et al., 2013; Sotiropoulos et al., 2012; Zhang et al., 2012), estimating properties like fiber density, fiber spread and fiber arrangement complexity.

Second, most of the commonly used tractography algorithms, both probabilistic (Behrens et al., 2003) and deterministic (Mori and van Zijl, 2002), are sequential procedures that suffer from error accumulation and increasing uncertainty especially over longer distances (Jones, 2010). In particular, weaker pathways that are dominated by larger crossing bundles may be difficult to reconstruct. A promising alternative is the use of global tractography techniques that do not iteratively integrate the local diffusion information, but instead use other principles, such as self organization of small elements (Fillard et al., 2009; Kreher et al., 2008; Reisert et al., 2011), Hough transform (Aganj et al., 2011) and the solution of the Hamilton–Jacobi–Bellman equation (Melonakos et al., 2007; Pichon et al., 2005). A particularly insightful and promising approach involves parameterized (usually spline based) representations of pathways between predefined endpoints, which are then fitted to the diffusion data (Jbabdi et al., 2007; Tuch, 2002). For a comparison of deterministic, probabilistic and global tractography, see (Bastiani et al., 2012).

The third problem of many current TBA methods lies in the fact that all long-range fiber-tracts have crossings with other tracts. Even if the tractography technique used can disentangle these crossings without problems, the mapped indices are not a good representation of the properties of the tract of interest anymore. This is especially relevant, if the volume fraction of the tract of interest is small, that is, if the crossing fibers dominate the diffusion signal. On the other hand, modern local models of the diffusion propagator (for example, *constrained spherical deconvolution* ((CSD); Tournier et al., 2007) allow, within certain limits, for the disentanglement of the properties of multiple crossing fiber populations and thereby enable the definition of direction dependent and bundle specific indices (Raffelt et al., 2012; Riffert et al., 2012, under review; Sotiropoulos et al., 2012). In consequence, in each voxel several indices may be available and one can select the one that belongs to the tract of interest and assess how well it corresponds to that tract.

Based on the above considerations, we developed a new global tractography method called plausibility tracking and use it in a framework for the non-invasive characterization of white matter fiber connections in the human brain. This framework allows characterizing axonal connections with fiber bundle specific indices that potentially provide more specific information about the tissue microstructure than indices of the diffusion tensor, but requires reliable local directions all along the pathway, which are provided by our new tractography method. Plausibility tracking describes, according to the underlying dMRI data, the most plausible pathway between two defined regions in the brain. In contrast to many existing tractography methods, it provides a reliable local direction of the fiber bundle of interest in every location. This allows using direction dependent and population specific local indices to be mapped onto the tract. Our hypothesis is that these indices provide a more specific characterization of the tissue microstructure along pathways than it would be possible with rotationally invariant indices. In order to keep our framework applicable to standard clinical and scientific settings, we here restrict ourselves to indices computed from single shell HARDI data, but other more sophisticated indices may be easily incorporated. As a result, we can characterize a particular connection between gray matter areas by its most likely pathway and by local estimates of microstructural traits while minimizing contamination by unrelated fiber populations. Moreover, plausibility tracking offers a convenient way to assess the appropriateness, or plausibility, of an estimated tract in the light of the data.

The paper is organized as follows. In the chapter Materials and methods we describe in detail the novelties and implementation of our framework. The Results section is subdivided into validation of the proposed tractography method and an application example, featuring comparison of direction dependent indices along the *inferior longitudinal fasciculus* (ILF) between children and adults. Finally, the method and results are discussed in the last chapter.

Materials and methods

Our method consists of six steps: dMRI preprocessing, local modeling, computation of indices, plausibility tracking, mapping of indices onto the fiber bundles and statistical evaluation.

For the validation of plausibility tracking on human data and the tract-based analysis, we used data from nine children (five girls, mean age 7.0 years, stddev 1.1) and nine adults (five female, 27.8 years, stddev 2.7) previously presented by Brauer et al. (2011, 2013). The data were acquired on a Siemens 3 T Trio scanner with 1.7 mm isotropic voxel size, GRAPPA acceleration factor 2, 3×60 diffusion directions and a b-value of 1000 s/mm^2 and 21 images without diffusion weighting (b0 images). Anatomical images were acquired with T1 and T2 in 1 mm resolution. All subjects were right handed and healthy. Written informed consent was obtained from the participants in accordance with the ethical approval from the University of Leipzig. Children gave verbal assent prior to scanning and written consent was obtained from their parent or guardian. In order to minimize effects due to different brain sizes, we chose adults with relatively small heads. A *t*-test revealed no significant difference in brain size between children and adults ($p = 0.45$).

Preprocessing

Before processing the data, dMRI volumes corrupted by movement of the participants were removed from the datasets. First, an automatic method was used to remove volumes of low quality. The algorithm was based on the fact that motion during the acquisition attenuates the signal in a slice. Usually the average voxel intensity of two consecutive slices (interleaved acquisition) does not change much. Only when motion extinguishes the signal in parts of a slice does its average voxel intensity differ greatly from its neighbors' and indicates corruption of the volume. In a following control step, visual inspection of the datasets ensured the satisfactory quality of the remaining data. The datasets used for further analysis have 185 to 198 out of 201 volumes.

Distortions from eddy currents were sufficiently suppressed by the double spin echo sequence used for the acquisition of the diffusion weighted images so that no explicit correction was necessary.

The complete analysis described in this publication was performed on 1 mm isotropic voxel size. We chose this resolution as a compromise between accuracy and speed, where all indices were computed in advance voxel by voxel and accessed through nearest-neighbor interpolation from then on. This reduces the computational cost of recurring interpolation during the optimization process (see below) dramatically, but provides finer grained information than the original 1.7 mm voxel size. To avoid multiple interpolation operations on the diffusion weighted images, motion correction, alignment with the MNI coordinate system (Collins et al., 1998) as well as interpolation to 1 mm isotropic voxel size were performed in a single step. Best results were achieved through the following protocol: perform motion correction on the original dMRI data using FSL (Smith et al., 2004; Woolrich et al., 2009) (http://fsl.fmrib.ox.ac.uk/fsl/fsl-4.1.9), separate background from the dMRI volumes and compute an FA map, rigidly align this FA map with an FA map (FMRIB58_FA_1mm.nii.gz) in MNI space and transform the average b0 image accordingly, align all dMRI volumes to the b0 image and correct the gradient vectors with the same transformation. This removed the volume-shifting and affine distortion effects of subject movements and resampled the diffusion data to 1 mm isotropic voxel size in one step. The eddy current distortions were sufficiently suppressed by the double spin echo sequence used for the acquisition so that no explicit correction was necessary.

The brain region was determined using FSL's brain extraction tool (bet). A Student's *t*-test revealed no significant difference in brain volume between children and adults ($p = 0.45$). The diffusion tensor indices FA, RD and AD were computed using the FSL software package (dtifit).

We defined a mask for the white matter region in order to restrict the analysis to that region. Standard approaches either apply a threshold on the FA map or compute a white matter probability map from the anatomical T1 weighted image. Here, we used a combined method. Due to non-linear distortions in the dMRI datasets caused by susceptibility artifacts, computing the white matter mask based on the T1 weighted image would result in a map that is not perfectly aligned with the diffusion data. Thresholding the FA map holds the risk of producing holes in crossing regions where the FA values are low. We applied SPM's segmentation algorithm (Ashburner and Friston, 2005) to the FA map. As the FA map is perfectly aligned with the diffusion data and the segmentation and registration algorithm incorporates not only intensity but also spatial information, this method results in highly reliable white matter probability maps that can be thresholded to obtain the white matter mask as shown in Fig. 1.

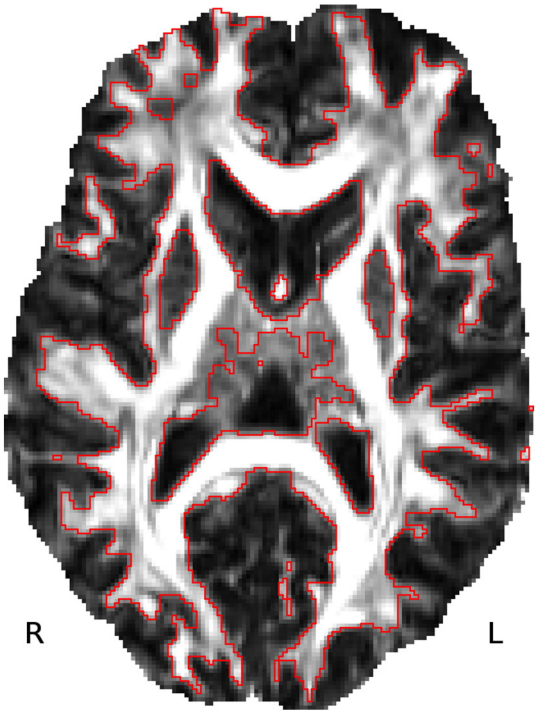

Fig. 1. Outline of the white matter mask obtained from segmentation of FA map.

Local modeling

We used CSD as implemented in MRtrix (Tournier et al., 2012) to compute the fODF (http://www.brain.org.au/software/mrtrix). In this approach, the fODF is obtained by deconvolving the diffusion signal attenuation with a kernel that represents the attenuation due to a population of parallel fibers. To regularize the results, CSD introduces a positivity constraint on the fODF amplitudes. Unlike methods approximating the diffusion propagator, (constrained) spherical deconvolution gives a measure that is directly related to the axonal fiber configuration (Leergaard et al., 2010; Leuze et al., 2014). For this approach it is necessary to have some knowledge of the signal attenuation that would be generated from completely parallel fibers (deconvolution kernel). The voxels that are used to compute this kernel response should be chosen from regions where all axonal fibers within one voxel run in the same direction. We computed a white matter skeleton for every individual subject based on its FA map using TBSS/FSL software (Smith et al., 2006). From this skeleton, only the 300 voxels with the highest FA within the given range (0.5–0.9) that were located within the corpus callosum region were chosen. The lower threshold ensured that the mono-directionality of the fibers and voxels with $FA > 0.9$ were removed because such high values indicate the possibility of being affected by an imaging artifact. In the following, we will call the voxels that are used to compute the kernel response kernel voxels.

In order to compare indices across subjects, a common kernel is required. Otherwise, subject specific characteristics might be coded into the kernel and neglected in the comparison. We computed the CSD coefficients for the kernel response directly from a tensor that is by definition axially symmetric. For the tensor, the principal eigenvalue λ_1 was calculated by the average of all λ_1 values of all kernel voxels averaged over all subjects. To ensure axial symmetry, the remaining eigenvalues λ_2 and λ_3 were set to the same value that was computed by averaging λ_2 and λ_3 of the kernel voxels. This led to the following configuration:

$$\lambda_1 = 0.0014 \quad \lambda_2 = \lambda_3 = 0.000177 \quad \Rightarrow \quad FA = 0.86 \quad MD = 0.0006\ .$$

Deviating from the protocol proposed by Tournier (http://www.brain.org.au/software/mrtrix/tractography/preprocess.html#csd), CSD was not performed on the diffusion-weighted signal but instead on the signal attenuation, which is required for the interpretation of the derived indices. The signal attenuation was obtained by dividing the diffusion-weighted images by the b0 image.

Indices based on Bingham functions fitted to the fODF

Indices based on Bingham fits to the fODFs were computed with CSD of order 6 and are compared with indices derived from the diffusion tensor. As shown by Descoteaux et al. (2009), applying CSD to dMRI data with a b-value of 1000 results in spurious peaks for higher orders than 6. All indices are computed for all subjects in the whole brain. The three largest fiber compartments of each voxel were used; smaller compartments were considered as noise and ignored.

The following indices proposed by Riffert et al. (under review) were used:

- The bundle specific *Fiber Density* (FD) is the integral of angular fiber densities and is computed by integrating the corresponding Bingham function. If the number of axons in the kernel voxels is known, FD can be measured absolutely in $\frac{1}{mm^3}$, otherwise FD represents the dimensionless relative fiber density compared to the kernel voxels.
- The *maximal Angular Fiber Density* (AFD_{max}) in a bundle is the local maximum of the fODF and is represented by the scaling parameter of the respective Bingham function. Similar to FD, AFD_{max} can be measured in $\frac{1}{mm^3 \cdot rad}$ or expressed as relative value in the unit $\frac{1}{rad}$. We do not directly analyze this index, but use it for the definition of Fiber Spread (see below).
- The *Fiber Spread* (FS) of a fiber bundle is measured indirectly and is defined as the ratio of FD and AFD_{max}:

$$FS_b = \frac{FD_b}{AFD^b_{\max}}. \quad (1)$$

It represents the angular width of a uniform distribution with the amplitude AFD_{max}. This opening angle can range between 0 and π.

- The *Fiber Fraction* (FF) describes how dominant (in terms of fiber density) the fiber bundle of interest is compared to all other fiber bundles in that location. For N (here $N \leq 3$) crossing-fiber bundles, the fiber fraction of the bundle of interest (b) is defined as

$$FF_b = \frac{FD_b}{\sum_{i=1}^{N} FD_i}. \quad (2)$$

To exemplify the relationship between these indices and the FA, four different fiber configurations extracted from real data are visualized as fODF glyphs and tensors (Fig. 2). The corresponding indices FD, FF, FS and FA are plotted for the two largest peaks. From the shape of the tensor and the corresponding FA values alone, it is not possible to distinguish between crossing and fanning fiber configurations. In contrast, the indices derived from the Bingham functions provide detailed information about the existence of minor fiber directions as well as the density and fanning of fibers within each fiber bundle. FD, FF and FS quantify the different parameters of the fiber bundle analog to the visual representation as glyphs.

If the real fiber density in the subjects' kernel voxels were known, it would be possible to multiply this number with the FD value to get an estimate of the biological fiber density in a bundle. Alternatively, a standard value of $3.717 \cdot 10^5$ fibers per mm^2 as published by Aboitiz et al. (1992) is used as approximation. As the absolute density of fibers is not known in our study and it is difficult to estimate due to missing information for children, FD is expressed relative to the FD in the kernel voxels.

Plausibility tracking

Plausibility tracking models the path of a fiber tract between two defined endpoints as a parameterized curve. The endpoints are fixed but the curve is optimized to describe the most plausible path through

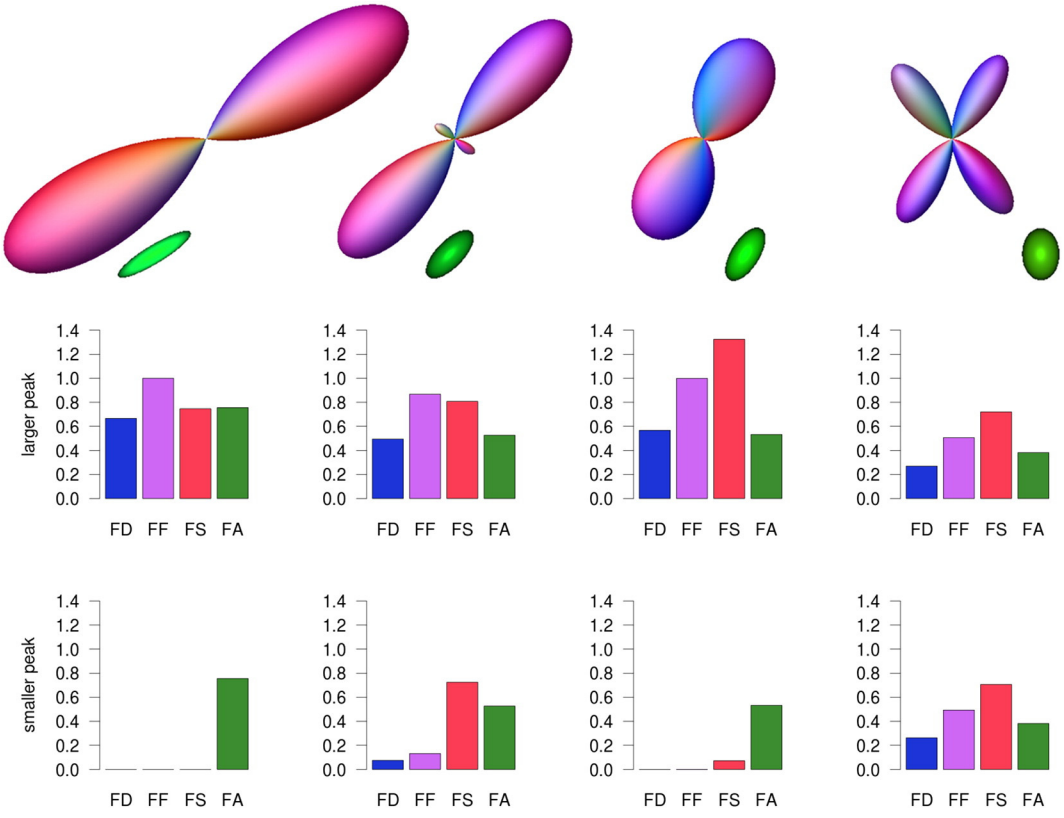

Fig. 2. Comparing indices of different fiber configurations. The top row shows glyphs (purple) and tensors (green) from different areas in the brain of an arbitrary participant. The second and third rows visualize the indices derived from Bingham fitting for the first and second peaks, respectively. To give a comparison, the FA values are visualized in both rows.

the brain. Possible axonal pathways are modeled with Catmull–Rom splines (Catmull and Rom, 1974). These are cubic splines that are parameterized solely by the location of control points and hence are fast and easy to optimize.

The control points can be divided into three different categories as visualized in Fig. 3. The first type comprises the two fixed locations on the gray–white matter interface whose connecting path is to be determined. In the optimization process, they are constants and not modified. The second category comprises the control points along the track. Their positions and number are flexible. A higher number of control points allows for a more accurate modeling of the path but also bears the risk of overfitting and increases processing time. Finally, there is a pair of two extra control points outside the curve that are required to define the curve's direction at the fixed end locations.

The speed and quality of finding the optimal parameters for the spline curve greatly depends on initialization. In the presented workflow, probabilistic tractography is used to get an estimate of the connecting pathway and to obtain the initial parameters by computing an average track. Deterministic streamline tractography is not suitable for this initialization because it follows only the most probable path and is not capable of describing connections through minor fiber bundles. Probabilistic tractography as described above determines the probability of two regions being connected and also finds connections that do not follow the major fiber bundles (Yo et al., 2009). By definition, the tracks obtained from probabilistic tractography are jagged and a single track does not necessarily reflect a possible axonal pathway. However, when taking into account multiple tracks that pass through two regions of interest, the majority of them follow the anatomically expected pathway.

Probabilistic tractography based on CSD is performed using the MRtrix software package (Tournier et al., 2012). In order to retrieve a set of probabilistic tracks that describe the connection of two locations in the brain, only those tracks that pass through both connection points within a defined radius r of 2.5 mm are selected. At least 11 tracks have to connect two points in order to render a connection significant. To compute the control points of a spline that describes the average of the N selected tracks $T = \{t_1,t_2,..,t_N\}$, a two-stage procedure is followed. First, each track $t_i \in T$ is parameterized along its arc length to define a fixed number M of regularly distributed track points $P_i = \{P_{i1}, P_{i2..}P_{iM}\}$. Second, the coordinates of the spline control points $C = \{c_1, c_2,..,c_M\}$ are computed by taking the medians of all corresponding track points. The fixed locations that are the endpoints of the curve define additional control points c_0 and c_{M+1} that will not be modified during the optimization process. Catmull–Rom splines are cubic splines that are described by the control points along their path plus two extra control points c_{-1} and c_{M+2} that define the direction at the fixed connection points c_0 and c_{M+1}. These two extra control points are initially set in the linear extrapolation of the fixed connection points and their neighboring control points. The computation of the control points is explained in Fig. 4.

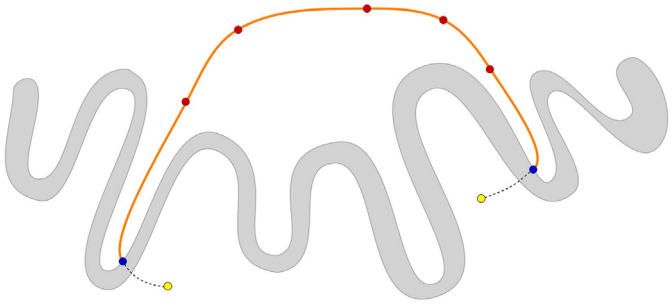

Fig. 3. Modeling the connecting pathway using Catmull–Rom splines. Three different types of control points define a pathway: the fixed end locations (blue), the control points on the path (red) and the two outer control points that define the direction (yellow) at the end locations.

After initialization, the spline parameters are optimized. This process consists of two major components: the metric to evaluate the quality of the current parameter set and the algorithm that chooses the next parameter set.

The metric in our method computes the current optimization value based on measurements from CSD. Spherical deconvolution has been chosen, because the local fODF values are, in theory, proportional to the density of axonal fibers with respect to the current local direction and hence provide the required information to estimate the plausibility of a pathway. Assuming that fibers are organized in bundles, the plausibility of a given local direction depends on the alignment with the bundle directions. The penalty for any deviation from the optimal peak direction depends on the spread of fibers within the bundle.

This is achieved by not using the absolute fODF amplitude $fODF\left(\vec{u}\right)$ in the current direction $\vec{u}$ but instead its value relative to its closest peak's $p\left(\vec{u}\right)$ amplitude $fODF\left(p\left(\vec{u}\right)\right)$. This provides a measure of local plausibility $\chi\left(\vec{u}\right)$ that can be described as

$$\chi\left(\vec{u}\right) = \frac{fODF\left(\vec{u}\right)}{fODF\left(p\left(\vec{u}\right)\right)}. \tag{3}$$

The computation of the local plausibility $\chi\left(\vec{u}\right)$ is shown in Fig. 5. As $fODF\left(\vec{u}\right)$ is by definition always smaller than or equal to the corresponding $fODF\left(p\left(\vec{u}\right)\right)$, the local plausibility $\chi\left(\vec{u}\right)$ ranges between 0 and 1. The maximal value is reached if the curve's local direction is perfectly aligned with one of the model's peak directions $p\left(\vec{u}\right)$. Any deviation from the closest peak's direction leads to smaller values, depending on the distribution of fiber directions modeled in the peaks. In peaks that represent strongly aligned fiber bundles and hence show a low spread, small directional deviations lead to strong decreases in the obtained value. Vice versa, $\chi\left(\vec{u}\right)$ decreases only moderately if the distribution of fiber directions is widespread and the glyphs have broad lobes. Even in peaks where the model was not able to distinguish two separate directions, reasonable values are obtained, because $\chi\left(\vec{u}\right)$ can be close to 1 even if the angle to the closest peak is relatively large (see Fig. 5). The fact that $fODF\left(\vec{u}\right)$ becomes 1 if $\vec{u}$ is perfectly aligned

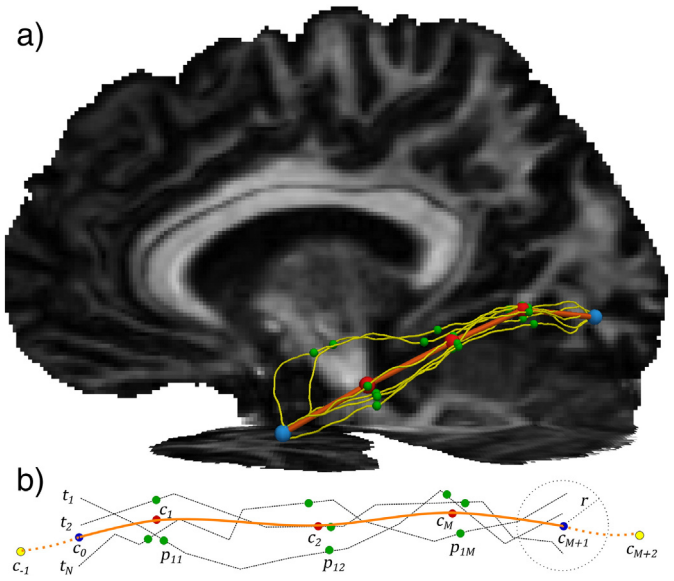

Fig. 4. Initialization based on probabilistic tractography. The method is visualized a) with real data and b) as a schematic drawing. Control points $\boldsymbol{c}$ for the Catmull–Rom splines are computed in a multi-stage procedure. Tracks $\boldsymbol{t}$ (yellow/black lines) are parameterized along their arc length to obtain track points p (green). The coordinates of corresponding track points $\boldsymbol{p}$ are then averaged to obtain spline control points $\boldsymbol{c}$ (red). Additional spline control points outside the track ($\boldsymbol{c_{-1}}$ and $\boldsymbol{c_{M+2}}$) (yellow) are placed in the linear prolongation of the endpoints $\boldsymbol{c_0}$ and $\boldsymbol{c_{M+1}}$ (blue).

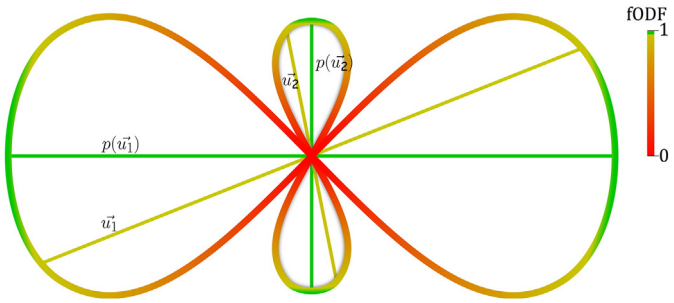

Fig. 5. Schematic drawing of a glyph with two peaks. The local plausibility value is computed as the ratio of the fODF values of the local fiber direction $\vec{u}$ (yellow) and its corresponding peak direction $\boldsymbol{p}(\vec{u})$ (green). The wider the peak, the slower the plausibility value decreases with deviation from the peak direction.

with *any* of the model's peak directions is coherent with our assumption that the plausibility of a fiber direction can also be maximal in minor fiber bundles.

In this context, the difference between probability and plausibility is that the probability of a track is high if it follows a pathway that potentially many fibers share. The plausibility of a track is characterized by a maximal accordance with local fiber directions. It is therefore proportional to the probability of the track orientation under the condition that the track belongs to a particular bundle (which can also be a minor one). Even in a highly unbalanced crossing, we consider it more plausible that a track continues a less dominant direction than bending sharply to follow the major fiber bundle.

The global plausibility X of a pathway is then computed as the average of all local plausibility values $X_i(\vec{u})$. As the initial parameters of the splines are already expected to be close to the optimum, a downhill optimization procedure can be used. Unfortunately, gradient information is not available to guide the optimizer because $\chi(\vec{u})$ is not always continuous. Therefore, we chose a downhill simplex optimization procedure (Nelder and Mead, 1965) that does not require gradients.

An optimization solely based on the global plausibility X is not advisable for two reasons. First, the path might produce loops with sharp bends. This is handled by adding a term Γ that penalizes excessive curvature of the path. Γ is defined as

$$\Gamma = \begin{cases} 1, & \text{if } \max(a_i(d)) < \frac{\pi}{4} \\ \exp\left(-\frac{1}{2\sigma^2}\left(\max\left(a_i(d) - \frac{\pi}{4}\right)\right)^2\right), & \text{if } \max(a_i(d)) \geq \frac{\pi}{4} \end{cases} \quad (4)$$

where $\alpha_i(d)$ is the angle between the tangents of two points on the curve with distance d (set to 5 mm) from the i-th of n points of the spline path and σ is set to π/4 and weights the influence of Γ. This penalizes bends if the angle between the two tangents becomes smaller than π/4. The Gaussian shape of the penalty function ensures a mild penalty for marginal undercuts of the given angle but pushes Γ close to 0 if the angle becomes much smaller.

Another constraint for the optimizer is set for the distribution of control points. Control points that are very closely spaced might cause looping artifacts or abrupt bends. In order to ensure a relatively homogenous distribution of control points, another term E has been added that constrains the minimum distance of two control points. It is defined as

$$E = 1 - \exp\left(-\frac{1}{2\sigma^2} \cdot \left(\frac{\min(D)}{\text{average}(D)}\right)^2\right) \quad (5)$$

where D is a set of distances between neighboring control points and σ being set to 0.2. Again, the Gaussian shape of this penalty function puts a mild penalty on small irregularities in the distribution of control points but pushes E close to 0 for a strong inhomogeneity in the distribution.

Furthermore, the pathway should not be allowed to leave the white matter area. However, just disqualifying the path as invalid when it leaves white matter does not provide the optimizer with any information in which direction to search for better parameter settings. Therefore, a modified plausibility measure $\chi^*(\vec{u})$ is defined as

$$\chi^*(\vec{u}) = \begin{cases} \chi(\vec{u}) & \text{if } \vec{u} \text{ is in white matter} \\ -\beta\left(1 - p_{wm}(\vec{u})\right) & \text{if } \vec{u} \text{ is not in white matter} \end{cases} \quad (6)$$

where $p_{wm}(\vec{u})$ is the probability of $\vec{u}$ being in white matter and β is a weighting factor that is set to 10. The decision, whether $\vec{u}$ is in white matter or not, is based on a thresholded map of white matter probability. This way, the number of points outside the white matter area and the distance to the gray–white matter boundary are taken into account.

The optimization value Ω for the path is then computed as

$$\Omega = -X^* \cdot \Gamma \cdot E. \quad (7)$$

The algorithm as described above has a number of parameters that have to be chosen. The values specified have been evaluated empirically when testing the algorithm on phantom data and different fiber pathways in the human brain. It turned out that the used values for the parameters of curvature, control point distribution and white matter probability are applicable for a wide range of fiber pathways. They provide a good compromise for straight and curved pathways and prevent loops as well as very sharp bends. By contrast, however, the search radius and the number of required probabilistic streamlines for the initialization as well as the number of control points depend very much on the pathway of interest. The number of required probabilistic streamlines also depends on the desired confidence that a connection is considered as real and the number of streamlines actually expected in each *region of interest* (ROI). The latter is similar to the unsolved problem at which value to threshold maps of probabilistic tractography. Visual inspection revealed that a minimum of 11 probabilistic streamlines is a good value for the given setup. The search radius ensures that streamlines that pass close by the defined coordinate can be considered for the connection. The larger the radius, the larger the number of required probabilistic streamlines should be. The number of control points depends on the complexity of the shape of the fiber pathway which is difficult to assess in advance. For specific fiber pathways, the number of control points can be assessed empirically. This can be seen in Figs. S1 and S2 of the supplementary data where several different fiber bundles have been reconstructed with described parameter values and the number of control points being the only parameter that has been adapted. When testing the plausibility of connection between a fixed location and various distributed other locations it turned out practical to estimate the length of the initial track and set control points every 15 or 20 mm (as done for Fig. 8).

Mapping indices onto the tracts

Having a local direction in every voxel along the connecting pathway makes it possible to analyze not only directionally invariant but also direction dependent indices. In order to compare locally corresponding quantities across subjects, two steps are necessary. First, the pathway of every subject has to be parameterized or segmented in a reproducible and comparable manner. Second, the indices have to be accumulated within their segments for statistical evaluation.

In the method presented here, the parameterization is performed with an extended version of Corouge's approach (Corouge et al., 2006). While these authors specify common start and endpoints by the intersection of the fiber tracts with two planes, we define multiple intersecting planes (as also suggested by Corouge) along the pathway and ensure the same number of evenly spaced samples per section across individuals. This procedure generates the same number of

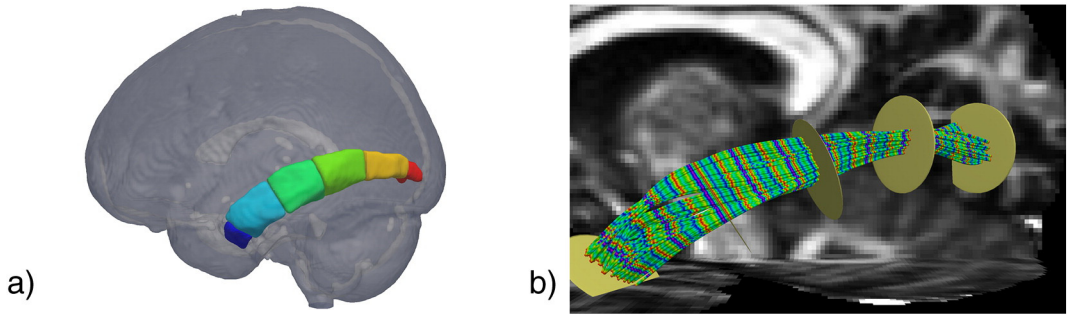

Fig. 6. Atlas and tracks of the left inferior longitudinal fasciculus of a single subject. a) The outer sections (blue and red) of an atlas define the areas for the fixed locations of the tracks (temporal pole and medial occipital lobe), while sampling of indices takes place only in the four central sections. b) Yellow disks represent the planes between the sections. The colored stripes on the track indicate corresponding samples that are summarized perpendicular to the pathway's main direction.

samples in every track in all subjects and ensures perpendicular correspondence of samples even along curved pathways. The planes are computed for every subject individually, guided by a purpose-built white matter volume atlas (see Fig. 6a) that is aligned[1] with each subject's anatomy. This atlas can be generated in any suitable way, depending on the available information. Here, it was constructed semi-automatically by manually defining seed and inclusion regions on the ILF on an MNI template (FMRIB58_FA_1mm.nii.gz). These regions were then transformed to each individual dataset by registration of the of the FA map with the MNI template. All probabilistic streamlines from whole brain tractography were extracted for each subject to get the probabilistic tracks of the ILF. These individual tracks were sampled to voxel maps which were then transformed back to MNI space and averaged. Thresholding and dilating the averaged track map resulted in a binary mask of the pathway. This mask was then divided manually into roughly equidistant sections, such that the sections are aligned with interesting features of the tracts, such as crossing areas. Finally the intersection planes for tract parameterization (Fig. 6b) were fitted to the boundaries between the sections using a support vector machine algorithm (Joachims, 1999).

Similar to Colby and colleagues (Colby et al., 2012), the values of indices along the pathway are sampled for every spline curve at a rate of 20 samples per atlas section (distance between successive points about 1 mm), thus dividing each section into 20 segments. As a consequence, voxel values from the index maps are potentially considered several times in the accumulation. This approach effectively causes a weighting of the index values: voxels that are passed more often by the modeled fiber tracks are considered to be more representative for the current connection and privileged accordingly.

There are three different types of indices that can be evaluated. In the simplest case, these are rotationally invariant and bundle-independent values (e.g. FA) that are sensitive to microstructural properties of the underlying tissue in every voxel. The second type comprises compartmental (i.e., one value per bundle) indices like FD, FS and FF. The third category of indices that can be evaluated with the presented method contains functions of the direction, like the amplitude of the fODF or the local plausibility as used for the plausibility tracking (see above).

Statistical evaluation of indices

As shown in Fig. 6b, the corresponding samples from all tracks of a subject form segments across the pathway. The measurement values at the sample locations are summarized by calculating the median for every segment. Consequently, for every index, the medians per segment and subject are calculated. As these median values are not necessarily normally distributed across subjects, we chose a non-parametric permutation test (Nichols and Holmes, 2002) that implicitly accounts for multiple comparisons. After writing the median values to an image file, we used the *randomise* tool implemented in the FSL software package (Smith et al., 2004; Woolrich et al., 2009) that performs the non-parametric randomization test. In addition, we also used post-processing by Threshold-Free-Cluster-Enhancement as described by Smith and Nichols (2009). Significance was defined for $p < 0.05$, resulting from two one-sided tests (as there is no a priori knowledge on the sign of the difference) at $p < 0.025$ and subsequent Bonferroni correction.

Application

The presented method was applied to two different fiber bundles. First, in order to demonstrate the explanatory power of the direction dependent indices, they were mapped onto an inter-hemispheric pathway connecting the left and right Brodmann Area 45 (Brodmann, 1909). Second, as in the example of the left *inferior longitudinal fasciculus* (ILF), we showed how differences between groups of subjects can be interpreted more specifically than with the widely used tensor derived indices.

Results

Plausibility tracking

For validation, plausibility tracking was applied to the phantom of the FiberCup (Fillard et al., 2011; Poupon et al., 2008) (http://www.lnao.fr/spip.php?rubrique79). This phantom shows various fiber configurations from parallel and bending to crossing and touching. The expected fiber pathways for this phantom are depicted in Fig. 7a.

For the evaluation of Plausibility Tracking, the data with a b-value of 1500 and a resolution of 3 mm^3 were used and interpolated to 1 mm^3. The deconvolution was performed with 6th order and the kernel is defined by a tensor with the following parameters:

$$\lambda_1 = 0.00184192 \quad \lambda_2 = \lambda_3 = 0.00111604 \quad \Rightarrow$$
$$FA = 0.2993 \quad MD = 0.001358\,.$$

These parameters were computed from the 37 voxels with highest FA. They differ significantly from those for human white matter because the diffusive properties of the plastic fibers used for the phantom are different from those of axons in the human brain.

In contrast to streamline tractography methods, it is not possible to start plausibility tracking in a single voxel and see where the track ends. hence, plausibility tracking was started in the spatial locations

[1] The registration task is performed with the Advanced Normalization Tools (ANTS http://www.picsl.upenn.edu/ANTS/) (Avants et al., 2008) that showed high class results in a comparison of different non-linear registration methods for atlas mapping (Klein et al., 2009). The FA map that corresponds to the atlas and the individual FA maps serve as basis for the registration as they are located natively in the diffusion space.

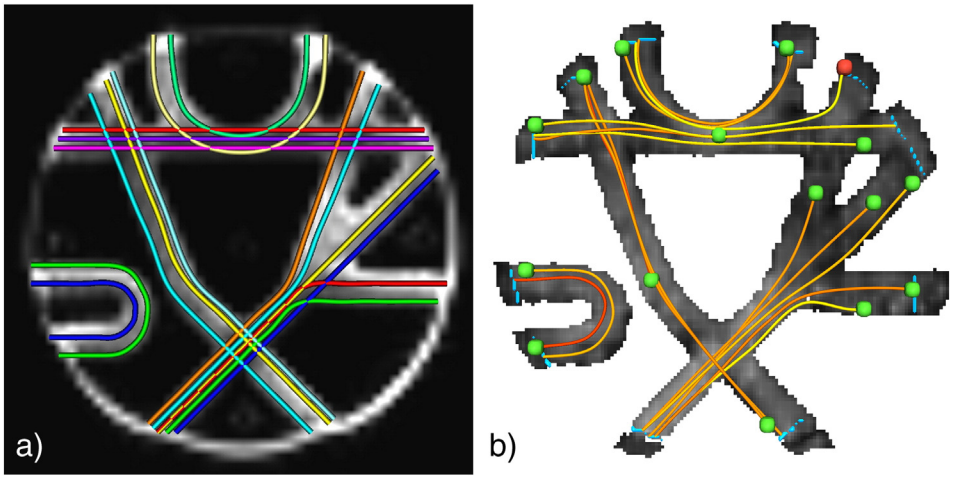

Fig. 7. Plausibility tracking applied to phantom data. a) Ground truth of fiber pathways as described by Fillard et al. (2011) b) Result from Plausibility Tracking. Every spatial location (green/red) is connected with the locations at the border (blue), only the most plausible pathway for every spatial location is displayed. Except for the spatial location that is colored red, all most plausible pathways are close to the ground truth.

suggested by the FiberCup and all voxels at the borders of the phantom were considered as possible connection points. This resulted in many tracks connecting every spatial location with multiple border voxels. For a comparison with streamline methods and the ground truth provided by the authors of the FiberCup, only the track with the highest plausibility for every seed location is selected and shown in Fig. 7b. In contrast to streamline methods, the tracks generated with plausibility tracking only track into a single direction so that all tracks where the spatial location is not placed at the border appears shorter than the ground truth in Fig. 7a. Except for one track (spatial location marked in red), all most plausible tracks follow the expected pathway.

A direct quantitative comparison with the methods, which participated in the FiberCup, is not possible because plausibility tracking is designed to find the pathway between two predefined regions and therefore follows only one direction from the starting point. Consequently, the scoring by the FiberCup's rating software would have been biased. However, plausibility tracking performs equally well to the global tractography method published by Reisert et al. (2009) and the FOD streamline method published by Jeurissen et al. (2009, 2011). These two methods clearly outscored the other methods at the FiberCup.

Plausibility tracking was also tested to connect different regions in the human brain. In order to evaluate the method, we compared it to both probabilistic and deterministic tractography, both implemented in MRtrix. We chose three separate points: *A* in the *prefrontal cortex* (PFC), within *Brodmann area 45* (BA45) and in the dorsal *motor cortex* (MC), all in the left hemisphere of a single subject. Then we computed the (according to the underlying dMRI data) most plausible connections with a large number of other points B_i covering the gray-white matter interface that was reached by probabilistic tractography, excluding locations of the same gyrus in which the corresponding A is located. In the case of A_{PFC}, points $B_{PFC,i}$ were limited to the right PFC to demonstrate the possibility to focus the analysis on distinct connections.

Plausibility tracks were initialized with a control point distance of 15 mm based on 25,000 probabilistic streamlines started in each of the voxels containing A_{PFC}, A_{BA45} and A_{MC}, respectively, while the deterministic streamlines were selected from whole-brain tractography performed with MRtrix based on CSD generating 250,000 tracks. In order to obtain a reasonable number of deterministic tracks, we selected those intersecting a sphere of radius 3.6 mm around the points A_{PFC}, A_{BA45} and A_{MC}, respectively. Constraining the spheres to the white matter led to effective volumes of 86 mm^3 (PFC), 149 mm^3 (BA45) and 178 mm^3 (MC).

Fig. 8 shows a comparison of probabilistic tractography, deterministic streamline tractography and Plausibility Tracking. Note that here, for the purpose of comparison, the probabilistic tractography is represented as a collection of streamlines rather than, as is common practice, a visitation map. This implies that no thresholding is applied. For some connections, the results of the three methods look quite similar for example when considering connections with A_{MC} as shown in Fig. 8. In other areas, it is possible to find connections in a much wider range using plausibility tracking compared to deterministic tractography. More specifically, plausibility tracking finds connections to more locations within a single target area as well as to more different target areas compared to deterministic tractography. For example, when studying the connections of the primary motor cortex (Fig. 8, middle row), plausibility tracking shows connections to large parts of both lateral and dorsal contralateral motor cortex, while deterministic tracking connects only a small spot in the lateral region, which is implausible both on anatomical and methodological grounds. Anatomically, such a one-to-one connection seems highly unlikely in the light of the complex motor actions to be executed. Methodologically, the uncertainty in the local models and the limited resolution of the data do not allow for such a precision of connectivity over a long distance (Jones et al., 2013). As a second example, for BA45, plausibility tracking recovers rich heterotopic transcallosal connections, which are likely to exist on the grounds of functional connectivity and lesion evidence (e.g., Turken and Dronkers, 2011), while deterministic tractography fails to reveal any transcallosal connection.

On the other hand plausibility tracking removes many tracks that obscure the fiber bundles in probabilistic tractography. These tracks may have low plausibility scores or do not connect the predefined regions. For example, for the tracks starting in the motor cortex (Fig. 8, middle row), there are clearly tracks jumping over to the cingulum and the *superior longitudinal fasciculus* (SLF), which is physiologically implausible. Likewise, for the BA45 and prefrontal starting points, probabilistic tractography seems to unspecifically connect almost the entire brain.

Unfortunately, lacking a comprehensive ground truth, it is not generally possible to tell exactly which tracks describe true fiber pathways in an individual subject and which tracks are false positives. However, it has been shown (Jones, 2008) that deterministic tractography is prone to missing out existing connections and that probabilistic tractography produces false positives. Potentially, plausibility tracking provides a reasonable compromise between false positive and false negative tracks. This assumption is supported by the results on the phantom data.

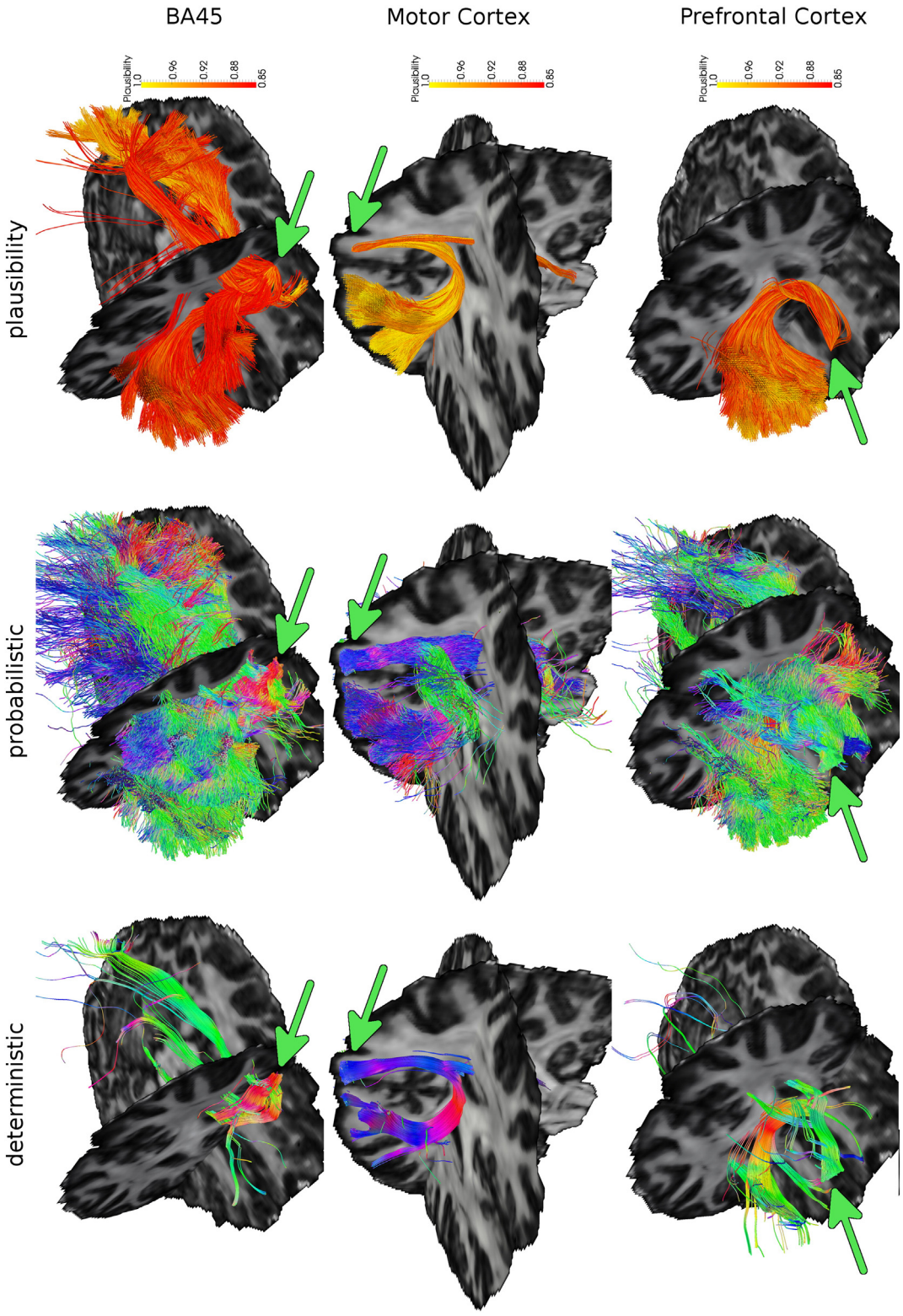

Fig. 8. Comparison of deterministic and probabilistic tractography with Plausibility Tracking. Plausibility tracking (right column) finds connections to a much wider range of areas than deterministic streamlines (left column) and shows much smoother and less noisy pathways than probabilistic tractography (middle column). As expected, in many cases the most plausible pathways coincide with the deterministic streamlines. Tracks with a plausibility (according to the underlying dMRI data) lower than 0.85 are not shown. Arrows indicate the seed regions. While the coloring of the plausibility tracking represents the plausibility values (according to the scale bar), the colors of the probabilistic and deterministic tractography results indicate the local streamline orientation in standard RGB color-coding.

Plausibility tracking found more existing connections than most deterministic streamline methods of the FiberCup but was able to eliminate false pathways.

Fig. 9 shows the probability distribution of plausibility values for the computed connections. In most cases the method is able to find very plausible connections for the selected pathways in the brain. The peak

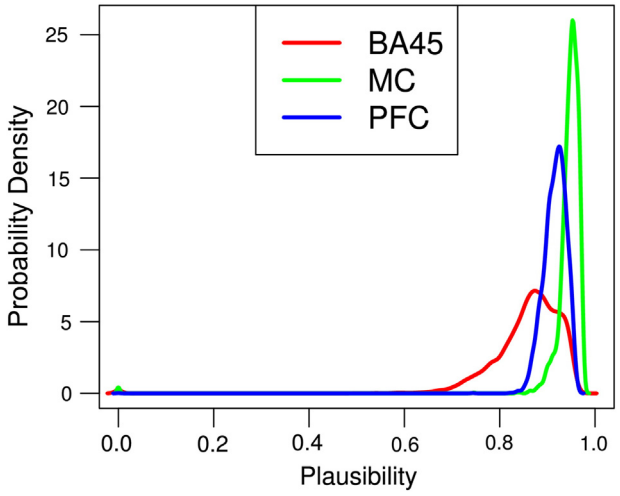

Fig. 9. Distribution of the plausibility of connections with point in BA45, MC and PFC. The graph shows a bi-modal distribution in all three examples.

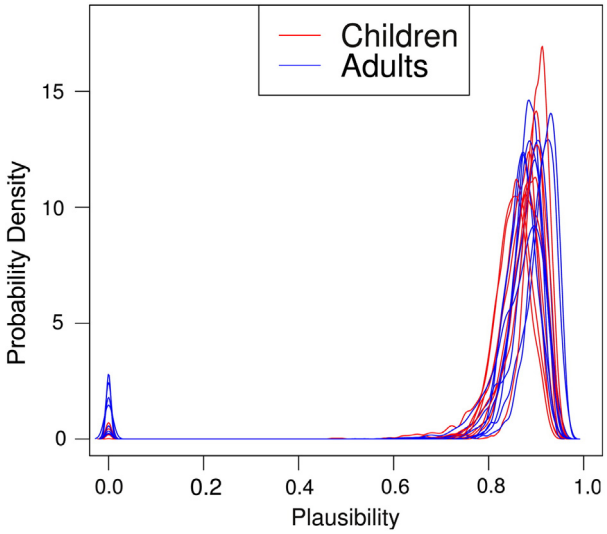

Fig. 11. Distribution of plausibility values plotted for the ILF of all subjects.

at a plausibility of zero is due to the fact that the track's plausibility is set to zero if the pathway leaves the white matter area even if only in a small fraction of the path. This strict criterion has been set to follow the premise that it is better to eliminate some correct tracks rather than accept questionable ones. To ensure comparability, the same plausibility threshold was used for all connections (0.85). With this threshold, a relatively small fraction of tracks is excluded (Fig. 9).

To compare direction dependent indices derived from CSD, plausibility tracking was applied to the ILF of all subjects. The ILF was defined by its end regions according to (Mori et al., 2008) and initialized with five control points evenly distributed on the pathway. Tracks with a plausibility value less than 0.75 were considered as implausible and excluded from the analysis. Fig. 10 shows the plausible tracks of the ILF color coded with their plausibility value.

In order to get an impression of the distribution of plausibility values within the pathway, Fig. 11 shows the probability densities of the track's plausibility values per subject. For some connections (0.4% in children and 1.7% in adults) the optimizer was not able to find a plausible pathway within the white matter area, but the majority of tracks reach a plausibility of more than 0.75. The strong bimodal distribution of plausibility values as visualized in Fig. 10 clearly shows that the optimizer is either able to find a very plausible pathway or fails completely, which makes it easy to decide which tracks one can trust. Only very few connections show intermediate plausibility values. In order to suppress questionable tracks, only those with a plausibility of at least 0.75 were considered for further analysis.

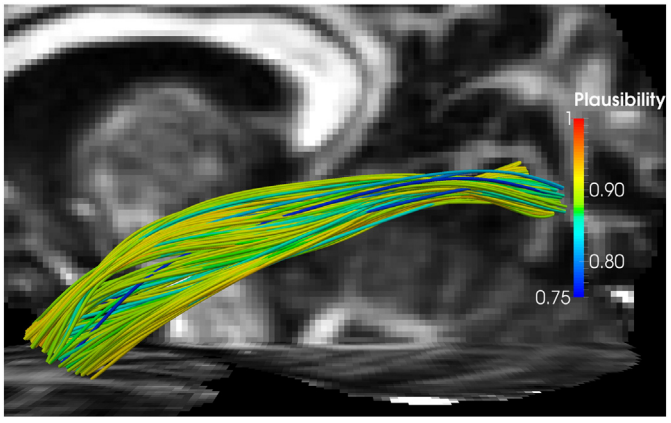

Fig. 10. Pathway of the left ILF modeled by plausibility tracking in one subject, overlaid to a sagittal slice of a FA map through the left occipital cortex. The tracks with a plausibility value greater than 0.75 are shown and color coded with their individual plausibility value.

Describing microstructural properties using Bingham derived indices

To show an example application of the presented method, indices derived from the fODF via Bingham functions are mapped onto an inter-hemispheric pathway between left and right BA45 that shows parallel, crossing and fanning fibers as shown in Fig. 12. As expected, FD and FF of this pathway are highest within the *corpus callosum* (CC), decrease to a minimum where they cross the SLF and the *corona radiata* (CR) and increase again slightly in the BA45 regions. We can assume that the compact fiber configuration in the corpus callosum widens in the crossing area to allow fibers from SLF and CR to intersect. Accordingly, FF decreases because not all fibers in this area belong to the fiber bundle of interest. In the gyri, FD and FF increase again as the fiber bundle compacts. Still, FD and FF do not reach the same level as in the corpus callosum as short association fibers and other gyral connections consume space. The value of FS supports this observation as it increases in the transition areas of different fiber densities. Coming from the CC, fibers are fanning out to intersect with the crossing-fiber bundles. The increase of FS in the middle of the CC may be explained with partial voluming with the septum pellucidum.

Comparing indices between groups

In a second experiment, Bingham derived indices are used in a group comparison study and placed in relation to indices of the diffusion tensor. All indices are mapped onto the individual pathways of the ILF (see Fig. 13) and accumulated separately for statistical evaluation.

In Fig. 14, Bingham derived indices (FD, FS and FF) and tensor derived indices (FA, AD, RD) are plotted as group medians along the left ILF from the temporal pole to the occipital region. The curves of FD and FA are remarkably similar, thus suggesting that the main factor influencing the FA in this region is the density of fibers in the main bundle. Consequently, they show a significant difference between children and adults at the same location on the pathway (as indicated by green shading). This significant difference emerges where fibers of the *inferior fronto-occipital fasciculus* (IFOF) and a transcallosal fiber bundle join the ILF within the temporal lobe, which can be seen nicely in Fig. 15.

Along the ILF, RD appears to be significantly higher in the group of children than in the adults within the anterior half of the ILF, which could be interpreted as areas of increased crossing and/or fanning of fibers compared to adults. The difference in AD is an observation that

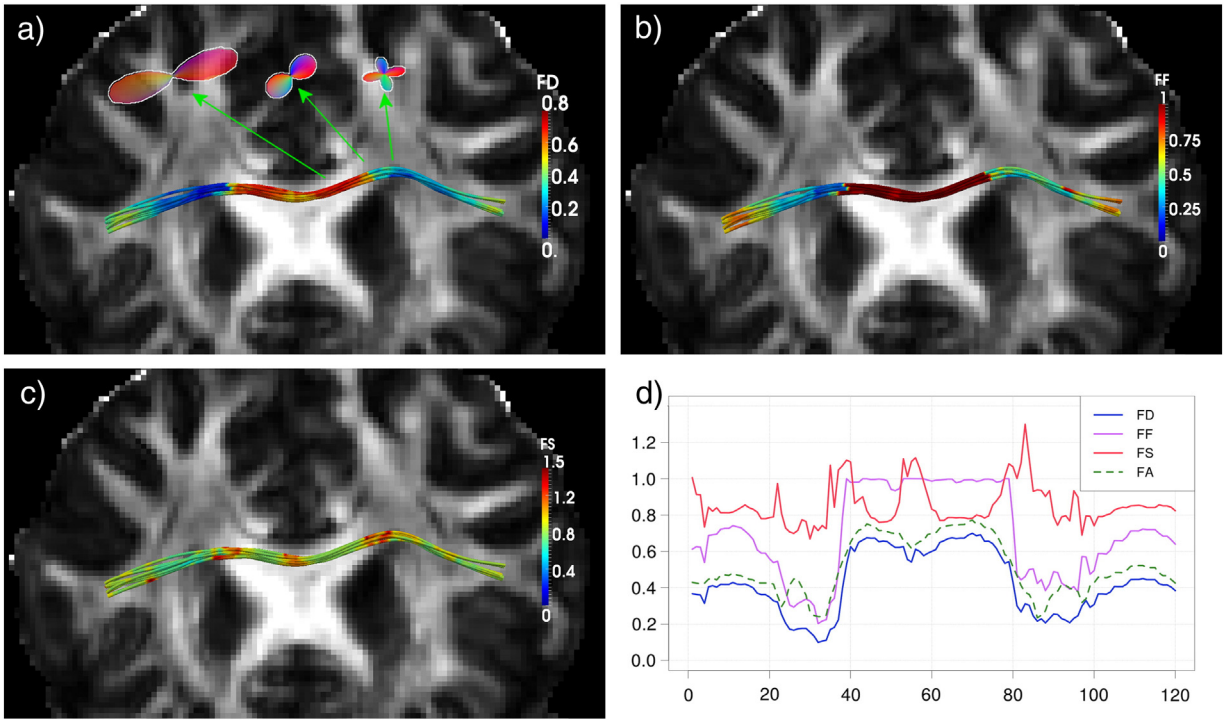

Fig. 12. Indices along the inter-hemispheric connection between left and right BA45, overlaid to a coronal slice of an FA map. It can be seen that FD (a) and FF (b) are highest in the corpus callosum and they show lowest values in the crossing areas. It is evident that FS (c) increases in the areas where the density of fibers changes. As a reference, the plot (d) also shows the values of FA which are quite similar to FD. Exemplary fODFs with different fiber configurations are visualized as glyphs in (a).

is probably impossible to interpret in this context. In contrast, indices FS and FF provide a little more solid ground for a hypothesis about the fiber configuration in this area. All along the temporal lobe where the ILF interacts with the IFOF and the transcallosal fibers, FS is higher in children than in adults suggesting that the fibers are spreading more in the younger subjects than in the adults. One possible reason for this effect might be the pruning of connections that are not well aligned with the ILF. In the area where group differences of FD and FA become obvious, another effect seems to dominate the fiber configuration: FF is significantly higher in adults compared to children, which suggests that the ILF maturates later than the crossing-fiber bundles in this area.

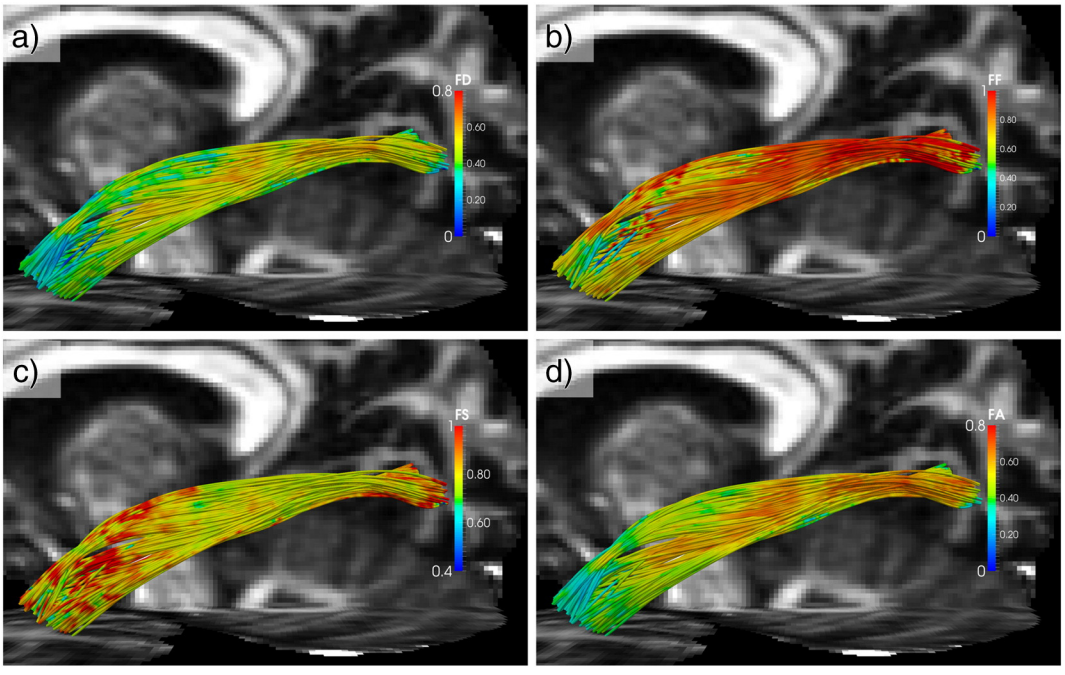

Fig. 13. Indices mapped onto the ILF pathway of a representative subject. a) Fiber density (FD); b) Fiber fraction (FF); c) Fiber spread (FS); d) Fractional anisotropy (FA).

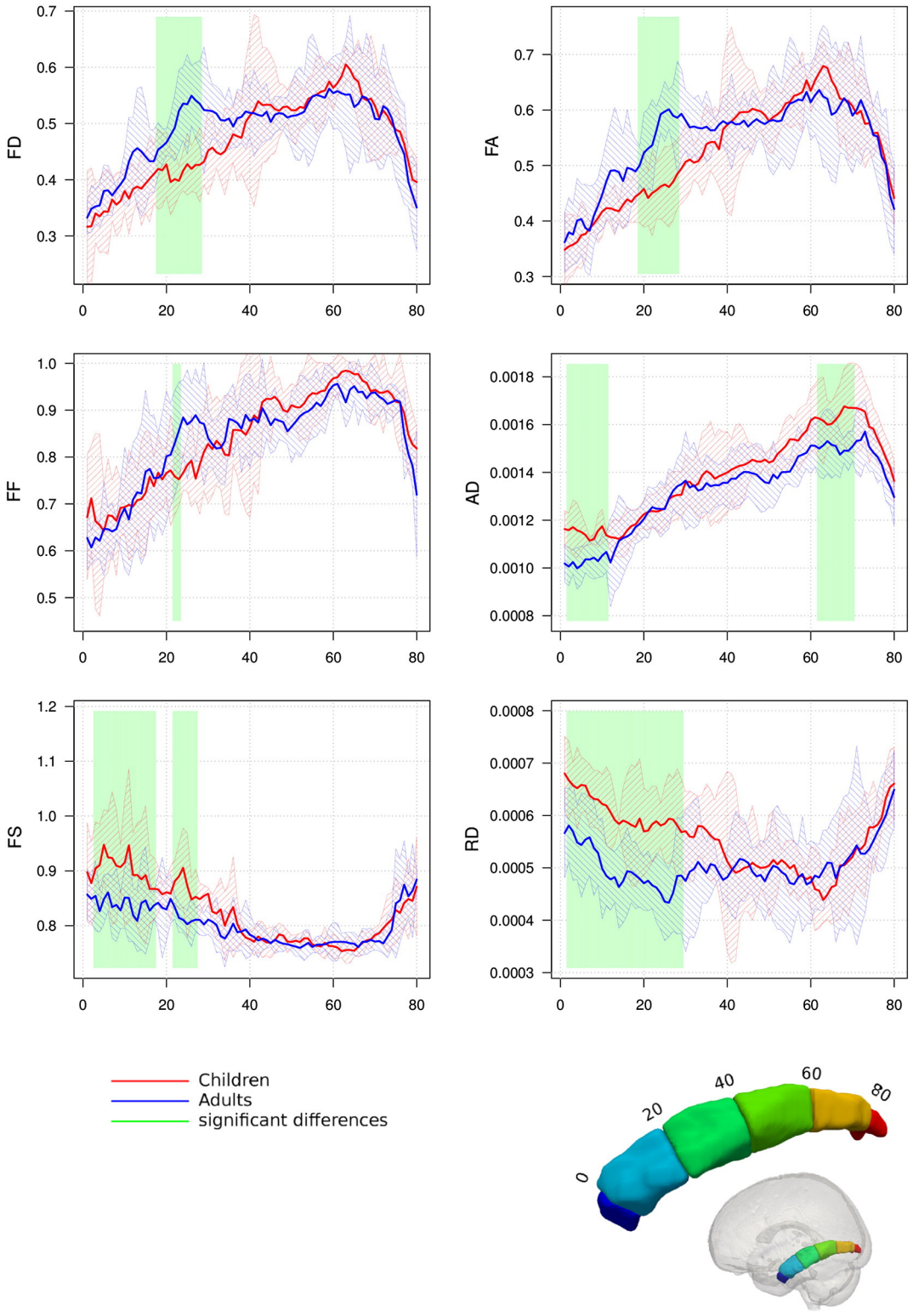

Fig. 14. Different indices sampled along the ILF. The median values are plotted separately for children (red) and adults (blue) from temporal (x = 0) to occipital (x = 80). The shaded red and blue areas show the variation within the groups, computed as 2 MAD (Median Absolute Deviation). The areas highlighted in green indicate significant differences between the groups ($p < 0.05$, corrected).

Discussion

Summary

We propose a new tractography method, called Plausibility Tracking, and demonstrate that it is able to reliably track different fiber bundles on phantom data as well as in the human brain. Plausibility tracking provides the most plausible pathway, modeled as a smooth spline curve, between two locations in the brain. The initialization based on probabilistic tractography keeps the computational cost low. The plausibility of a connection is defined by the accordance of the track's directions with the local directions and their uncertainties measured with

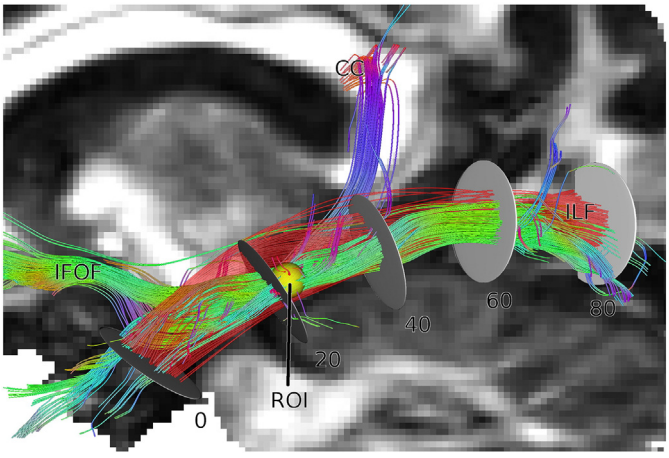

Fig. 15. Fiber bundles interacting with the ILF within the temporal lobe. Tracks of deterministic streamline tractography that cross the ROI (yellow) are visualized together with the plausibility tracks of the ILF (red, transparent) and the planes that separate the sections of the atlas (gray disks).

dMRI. Plausibility tracking combines the more complete connectivity pattern provided by probabilistic tractography techniques with smooth tracks that are globally optimized using the fiber orientation density function and hence is relatively robust against local noise and error propagation. Most importantly, the smooth curve of plausibility tracking and the optimization to the most plausible pathway make it suitable for demanding applications like tract-based analysis with fiber bundle specific indices. To demonstrate this, we developed a framework to compare direction dependent indices derived from dMRI across subjects. Defined through fitting a Bingham function to the fODFs generated with CSD, FD, FS and FF are fiber bundle specific indices that are compared to tensor derived indices. Plausibility tracking is used to obtain reliable local directions in the fiber bundles. We showed that the proposed method allows for a more specific interpretation of the white matter's microstructure compared to rotationally invariant indices derived from the diffusion tensor.

Plausibility tracking

In contrast to previously published methods of curve fitting (Jbabdi et al., 2007; Tuch, 2002), plausibility tracking is initialized by probabilistic tractography that produces a good estimate of the initial spline parameters. With this initialization, a fast gradient descent algorithm can be used and finds the global optimum very quickly. Outliers from the initial probabilistic tractography have little impact on the outcome of the final Plausibility Tracking, as a two stage filter is implicitly implemented. First, multiple probabilistic tracks are required to initialize a pathway so that connections with low probability (i.e., with very few probabilistic tracks) are ignored. Second, the estimation of the spline parameters acts as a filter itself because connections that are implausible in the light of the diffusion data obtain a low plausibility value and are removed. Additional post-processing methods like the recently introduced *spherical-deconvolution informed filtering of tractograms* (SIFT) (Smith et al., 2013) could be applied.

The measure of plausibility is based solely on the agreement with the direction and uncertainty of one of the peaks described by the local model, although the optimization process uses additional terms regarding curvature constraints and control point distribution. In this sense, *plausibility* denotes how well the local directions can be explained by the local model and assumes that the local model describes the underlying fiber configuration completely. In practice, this requirement is not fulfilled and can never be fully fulfilled due to technical limitations and the indirect estimation of the fODF (Jones et al., 2013). However, the model has been regarded accurate enough to evaluate properties of differences in white matter tissue (Raffelt et al., 2012). On the other hand, the framework proposed here can be applied to any type of higher order local model.

Another assumption that has direct influence on the plausibility has been made regarding the smoothness of the pathway. This smoothness is introduced by modeling the pathway by a spline curve with a limited number of control points and forcing the optimizer to avoid sharp bends. Modeling axonal pathways with a smooth curve might appear questionable, as axons cannot be expected to always follow a smooth curve but may show abrupt changes in direction in certain areas. On the other hand, although dMRI is performed at reasonably high resolution, it still summarizes the signal of thousands of axons within one voxel. Hence, the 'true' axonal pathway is out of reach of dMRI and the assumption of smoothness refers to the average path of thousands of axons. The method presented here uses a global constraint for smoothness in the whole brain, which is a compromise that prevents implausible bends, but still allows modeling of curved pathways. Within the framework, it would also be possible to create an atlas with expected local curvature angles and adapt the constraint for smoothness locally.

In order to reduce partial volume and obtain more detailed information about separate local fiber directions one may consider employing latest ultra-high field MR scanners with resolution-optimized protocols as introduced by Heidemann et al. (2010, 2012). When using higher spatial resolution data, the number of control points that define the spline can be increased accordingly.

The track's global plausibility value is computed as the average of all local plausibility values sampled along the pathway. The effect that this simple definition has on local deviations from the optimal direction can be compensated for by sections with good directional accordance with the local model. Accordingly the track's length does not have an impact on its plausibility value. Compensating for locally implausible situations poses the risk of constructing pathways that are biologically impossible like taking a shortcut through non-white matter areas. In order to prevent these cases, a strict criterion has been set to disregard any pathway that leaves white matter.

A visual comparison with other methods of tractography was performed based on a phantom with synthetic fibers (Fillard et al., 2011), where the ground truth of the fiber pathways is known. It showed that plausibility tracking provides similar results to the two best methods in the FiberCup competition. Plausibility tracking was able to track 15 out of 16 pathways as expected. The one track that did not follow the real fiber pathway failed already in the process of initialization. In that case, most of the probabilistic tracks followed the same false route as the probabilistic tracks shown in the supplementary material of the publication related to the FiberCup (Fillard et al., 2011), although different methods of probabilistic tractography (Behrens et al., 2007; Tournier et al., 2012) have been used.

TBA in contrast to other white matter mapping methods

Standard mapping methods like *voxel-based analysis* (VBA) (Ashburner and Friston, 2000) and *region* or *atlas-based analysis* (Faria et al., 2010; Snook et al., 2007) are able to handle only rotationally invariant indices. Also the *tract-based spatial statistics* (TBSS, http://fsl.fmrib.ox.ac.uk/fsl/fslwiki/TBSS) method (Smith et al., 2006) has originally been developed to analyze indices derived from the diffusion tensor, but has been extended by Jbabdi and colleagues (Douaud et al., 2011; Jbabdi et al., 2010) to handle direction dependent *partial volume fractions* (PVF) and, potentially, indices of other crossing-fiber models. Raffelt et al. (2012) perform a voxel-based comparison of the fiber orientation density at 200 sampled orientations. All these methods indicate the location in the brain where differences between groups occur, but they do not directly show which fiber pathways or connections are affected or what the anatomical discrepancy might be.

While with TBSS and VBA the whole brain is analyzed by default, only distinct pathways are evaluated with TBA. This can be done by either first mapping the index values onto the fiber tracts and then transforming the tracts to a common coordinate system to allow a voxel-wise comparison between brains without interpolation effects (Ros et al., 2012) or by parameterizing the tractography streamlines along their arc length and summarizing the indices according to their position between the two regions of interest. The difficulty with the latter approach is that the definition of correspondences along the tract is not trivial. Several solutions to this have been proposed (Colby et al., 2012; Corouge et al., 2006; Gong et al., 2005; O'Donnell et al., 2009) that all measure absolute or relative distances, either on some central line or on all streamlines. As many fiber tracts in the brain have a rather sheet-like appearance, Yushkevich et al. (2008) model sheet-like tracts by medial representation to reduce data dimensionality and average tensor-based features onto the medial representation. For the method presented here, the user not only has to choose a pathway of interest, but also, if it does not already exist, create a suitable atlas. The advantage of this slightly more laborious approach is that one obtains more specific information on distinct fiber bundles even where they are intersected by more dominant ones.

TBSS is based on a skeleton of maximal FA and therefore inadequately represents areas with characteristically low FA, such as crossing. In addition, the limitation to the center line of the white matter with maximal FA gives rise to a bias in the estimated bundle properties. VBA on the other hand does not explicitly concentrate on high FA values, but comes along with a strong smoothing that is prone to hiding local variances in the tissue's structure and changes the statistics (Jones et al., 2005). In contrast, the TBA method proposed in this article reduces smoothing to a minimum (caused by motion correction), keeping the individual data as unbiased as possible. It allows the analysis of connections realized through minor fiber bundles as well as the major tracts and separates the dMRI information from different tracts. In contrast to previously published methods of TBA (Colby et al., 2012; Corouge et al., 2006; Lebel et al., 2008), our method allows us to analyze direction dependent indices along the tract that, as has been shown, have the potential to give more specific information about the underlying fiber structure than rotationally invariant indices.

Mapping of indices

It is common standard in TBA to pool index values according to the parameterization along the pathway (Colby et al., 2012; Corouge et al., 2006). The atlas-based definition of supporting planes, as described in this paper, increases the comparability between subjects as the spatial normalization process for the atlas takes characteristics in the individual anatomies into account. Due to the fact that only the atlas is transformed to the individual space and not the diffusion data or index maps themselves, no smoothing artifacts from interpolation are expected.

Tensor based indices, such as *fractional anisotropy* (FA), *mean diffusivity* (MD), *axial diffusivity* (AD) and *radial diffusivity* (RD) (Basser, 1995; Song et al., 2002) have been used prevalently in a large number of neuroimaging studies. The diffusion tensor is, strictly speaking, not suitable to model voxels within crossing-fiber regions (Alexander et al., 2001, 2002; Tuch et al., 2002). Nonetheless, such indices have been used to gain insight into a wide range of brain diseases and cognitive faculties (see Jones et al., 2013 for a review). This has been possible because FA is indeed very sensitive to changes or anomalies in the brain's white matter. On the other hand, the measure is not very specific and does not reveal unambiguously which microstructural constellation leads to a certain value. Jbabdi et al. (2007) illustrate elegantly the challenge faced when attempting to interpret a change in FA in crossing-fiber regions. See also the review by Jones et al. (2013) for a critical discussion. More sophisticated scalar measures can be based on advanced local models, such as the generalized fractional anisotropy (Tuch, 2002), but also these indices cannot distinguish between the contributions of different fiber bundles.

In the present study, direction dependent indices, as recently introduced by Riffert et al. (under review), were used to identify properties of the white matter structure. Fitting a Bingham function into the peaks of the fODF is an elegant way to obtain direction dependent indices from CSD. Even if the Bingham function does not always fit perfectly to the fODF, Riffert et al. (under review) showed that the error of the derived indices is within acceptable limits. These indices assume that the general tissue properties are constant within the white matter and that the only parameter that changes is the angular fiber density. While this assumption might be considered as fulfilled in healthy subjects, it becomes questionable in cases of diseases where the tissue structure is influenced by loss of myelin, edema or other factors. Computing local deconvolution kernels for every voxel might be the solution, but it would require some independent information on the fiber properties.

We showed that indices based on Bingham functions have more explanatory power than the widely used tensor indices. They are based on a single-b-value recording scheme that is suitable for a wide range of research facilities and clinical setups. However, in the framework proposed here, other types of indices can also be used. In fact, the full potential of the presented method will unfold when additional indices based on models like CHARMED (Assaf et al., 2004) and the axon diameter distribution (Assaf et al., 2008; Zhang et al., 2011a, 2011b) are used, which embody a more complete sampling of the diffusion propagator might bring even more insights into myelination or axonal diameter distribution. The other important route to improvement, especially for the tractography part of the framework, may be the increase of spatial resolution, which reduces partial volume effects (Heidemann et al., 2012). It also might be possible to combine information from the pathway's shape, like the area of cross-section, with the axonal density to estimate the actual number of axons along the pathway.

Supplementary data to this article can be found online at http://dx.doi.org/10.1016/j.neuroimage.2014.01.002.

Acknowledgments

Part of this work was supported by the FET project CONNECT of the EU (www.brain-connect.eu).

References

Aboitiz, F., Scheibel, A.B., Fisher, R.S., Zaidel, E., 1992. Fiber composition of the human corpus callosum. Brain Res. 598, 143–153.
Aganj, I., Lenglet, C., Sapiro, G., Yacoub, E., Ugurbil, K., Harel, N., 2010. Reconstruction of the orientation distribution function in single- and multiple-shell q-ball imaging within constant solid angle. Magn. Reson. Med. 64, 554–566.
Aganj, I., Lenglet, C., Jahanshad, N., Yacoub, E., Harel, N., Thompson, P.M., Sapiro, G., 2011. A Hough transform global probabilistic approach to multiple-subject diffusion MRI tractography. Med. Image Anal. 15, 414–425.
Alexander, D.C., 2005. Multiple-fiber reconstruction algorithms for diffusion MRI. Ann. N. Y. Acad. Sci. 1064, 113–133.
Alexander, A.L., Hasan, K.M., Lazar, M., Tsuruda, J.S., Parker, D.L., 2001. Analysis of partial volume effects in diffusion-tensor MRI. Magn. Reson. Med. 45, 770–780.
Alexander, D.C., Barker, G.J., Arridge, S.R., 2002. Detection and modeling of non-Gaussian apparent diffusion coefficient profiles in human brain data. Magn. Reson. Med. 48, 331–340.
Alexander, D.C., Hubbard, P.L., Hall, M.G., Moore, E.A., Ptito, M., Parker, G.J.M., Dyrby, T.B., 2010. Orientationally invariant indices of axon diameter and density from diffusion MRI. NeuroImage 52, 1374–1389.
Anwander, A., Tittgemeyer, M., von Cramon, D.Y., Friederici, A.D., Knösche, T.R., 2007. Connectivity-based parcellation of broca's area. Cereb. Cortex 17, 816–825.
Ashburner, J., Friston, K.J., 2000. Voxel-based morphometry — the methods. NeuroImage 11, 805–821.
Ashburner, J., Friston, K.J., 2005. Unified segmentation. NeuroImage 26, 839–851.
Assaf, Y., Freidlin, R.Z., Rohde, G.K., Basser, P.J., 2004. New modeling and experimental framework to characterize hindered and restricted water diffusion in brain white matter. Magn. Reson. Med. 52, 965–978.
Assaf, Y., Blumenfeld-Katzir, T., Yovel, Y., Basser, P.J., 2008. AxCaliber: a method for measuring axon diameter distribution from diffusion MRI. Magn. Reson. Med. 59, 1347–1354.

Avants, B., Epstein, C., Grossman, M., Gee, J., 2008. Symmetric diffeomorphic image registration with cross-correlation: evaluating automated labeling of elderly and neurodegenerative brain. Med. Image Anal. 12, 26–41.

Basser, P.J., 1995. Inferring microstructural features and the physiological state of tissues from diffusion-weighted images. NMR Biomed. 8, 333–344.

Basser, P.J., Pierpaoli, C., 1996. Microstructural and physiological features of tissues elucidated by quantitative-diffusion-tensor MRI. J. Magn. Reson. B 111, 209–219.

Basser, P.J., Mattiello, J., LeBihan, D., 1994. Estimation of the effective self-diffusion tensor from the NMR spin echo. J. Magn. Reson. B 103, 247–254.

Bastiani, M., Shah, N.J., Goebel, R., Roebroeck, A., 2012. Human cortical connectome reconstruction from diffusion weighted MRI: the effect of tractography algorithm. NeuroImage 62, 1732–1749.

Beaulieu, C., 2002. The basis of anisotropic water diffusion in the nervous system—a technical review. NMR Biomed. 15 (7–8), 435–455.

Behrens, T.E.J., Woolrich, M.W., Jenkinson, M., Johansen-Berg, H., Nunes, R.G., Clare, S., Matthews, P.M., Brady, J.M., Smith, S.M., 2003. Characterization and propagation of uncertainty in diffusion-weighted MR imaging. Magn. Reson. Med. 50, 1077–1088.

Behrens, T.E.J., Berg, H.J., Jbabdi, S., Rushworth, M.F.S., Woolrich, M.W., 2007. Probabilistic diffusion tractography with multiple fibre orientations: what can we gain? NeuroImage 34, 144–155.

Brauer, J., Anwander, A., Friederici, A.D., 2011. Neuroanatomical prerequisites for language functions in the maturing brain. Cereb. Cortex 21, 459–466.

Brauer, J., Anwander, A., Perani, D., Friederici, A.D., 2013. Dorsal andventral pathways in language development. Brain Lang 127 (2), 289–295.

Brodmann, K., 1909. Vergleichende Lokalisationslehre der Großhirnrinde. Barth, Leipzig.

Catmull, E., Rom, R., 1974. A Class of Local Interpolating Splines. Computer Aided Geometric Design. Academic Press 317–326.

Colby, J.B., Soderberg, L., Lebel, C., Dinov, I.D., Thompson, P.M., Sowell, E.R., 2012. Along-tract statistics allow for enhanced tractography analysis. NeuroImage 59, 3227–3242.

Collins, D.L., Zijdenbos, A.P., Kollokian, V., Sled, J.G., Kabani, N.J., Holmes, C.J., Evans, A.C., 1998. Design and construction of a realistic digital brain phantom. IEEE Trans. Med. Imaging 17, 463–468.

Corouge, I., Fletcher, P.T., Joshi, S., Gouttard, S., Gerig, G., 2006. Fiber tract-oriented statistics for quantitative diffusion tensor MRI analysis. Med. Image Anal. 10, 786–798.

Dell'Acqua, F., Rizzo, G., Scifo, P., Clarke, R.A., Scotti, G., Fazio, F., 2007. A model-based deconvolution approach to solve fiber crossing in diffusion-weighted MR imaging. IEEE Trans. Biomed. Eng. 54, 462–472.

Dell'Acqua, F., Simmons, A., Williams, S.C., Catani, M., 2013. Can sphericaldeconvolution provide more information than fiber orientations? Hindrancemodulated orientational anisotropy, a true-tract specific index tocharacterize white matter diffusion. Hum. Brain Mapp 34 (10), 2464–2483.

Descoteaux, M., Deriche, R., Knösche, T.R., Anwander, A., 2009. Deterministic and probabilistic tractography based on complex fibre orientation distributions. IEEE Trans. Med. Imaging 28, 269–286.

Douaud, G., Jbabdi, S., Behrens, T.E.J., Menke, R.A., Gass, A., Monsch, A.U., Rao, A., Whitcher, B., Kindlmann, G., Matthews, P.M., Smith, S., 2011. DTI measures in crossing-fibre areas: increased diffusion anisotropy reveals early white matter alteration in MCI and mild Alzheimer's disease. NeuroImage 55, 880–890.

Faria, A.V., Zhang, J., Oishi, K., Li, X., Jiang, H., Akhter, K., Hermoye, L., Lee, S.-K., Hoon, A., Stashinko, E., Miller, M.I., van Zijl, P.C.M., Mori, S., 2010. Atlas-based analysis of neurodevelopment from infancy to adulthood using diffusion tensor imaging and applications for automated abnormality detection. NeuroImage 52, 415–428.

Fillard, P., Poupon, C., Mangin, J.-F., 2009. A novel global tractography algorithm based on an adaptive spin glass model. Proc Med Image Comput Comput Assist Interv, vol. 1. MICCAI, London, UK 927–934.

Fillard, P., Descoteaux, M., Goh, A., Gouttard, S., Jeurissen, B., Malcolm, J., Ramirez-Manzanares, A., Reisert, M., Sakaie, K., Tensaouti, F., et al., 2011. Quantitative evaluation of 10 tractography algorithms on a realistic diffusion mr phantom. NeuroImage 56, 220–234.

Frank, L.R., 2002. Characterization of anisotropy in high angular resolution diffusion-weighted MRI. Magn. Reson. Med. 47, 1083–1099.

Gong, G., Jiang, T., Zhu, C., Zang, Y., Wang, F., Xie, S., Xiao, J., Guo, X., 2005. Asymmetry analysis of cingulum based on scale-invariant parameterization by diffusion tensor imaging. Hum. Brain Mapp. 24, 92–98.

Heidemann, R.M., Porter, D.A., Anwander, A., Feiweier, T., Heberlein, K., Knösche, T.R., Turner, R., 2010. Diffusion imaging in humans at 7 T using readout-segmented EPI and GRAPPA. Magn. Reson. Med. 64, 9–14.

Heidemann, R.M., Anwander, A., Feiweier, T., Knösche, T.R., Turner, R., 2012. k-space and q-space: combining ultra-high spatial and angular resolution in diffusion imaging using ZOOPPA at 7 T. NeuroImage 60, 967–978.

Jbabdi, S., Woolrich, M.W., Andersson, J.L.R., Behrens, T.E.J., 2007. A Bayesian framework for global tractography. NeuroImage 37, 116–129.

Jbabdi, S., Behrens, T.E.J., Smith, S.M., 2010. Crossing fibres in tract-based spatial statistics. NeuroImage 49, 249–256.

Jeurissen, B., Leemans, A., Tournier, J.D., Sijbers, J., 2009. Fiber tracking on the 'fiber cup phantom' using constrained spherical deconvolution. MICCAI Workshop on Diffusion Modelling and the Fiber Cup (DMFC'09), London, United Kingdom.

Jeurissen, B., Leemans, A., Jones, D.K., Tournier, J.-D., Sijbers, J., 2011. Probabilistic fiber tracking using the residual bootstrap with constrained spherical deconvolution. Hum. Brain Mapp. 32, 461–479.

Joachims, T., 1999. Making large-scale SVM learning practical. In: Schölkopf, B., Burges, C., Smola, A. (Eds.), Advances in Kernel Methods — Support Vector Learning. MIT Press, Cambridge, USA, pp. 169–184.

Jones, D.K., 2008. Studying connections in the living human brain with diffusion MRI. Cortex 44, 936–952.

Jones, D.K., 2010. Challenges and limitations of quantifying brain connectivity in vivo with diffusion MRI. Imaging 2 (3), 341–355.

Jones, D.K., Symms, M.R., Cercignani, M., Howard, R.J., 2005. The effect of filter size on VBM analyses of DT-MRI data. NeuroImage 26, 546–554.

Jones, D.K., Knösche, T.R., Turner, R., 2013. White matter integrity, fiber count, and other fallacies: the do's and don'ts of diffusion MRI. NeuroImage 73, 239–254.

Kaden, E., Knösche, T.R., Anwander, A., 2007. Parametric spherical deconvolution: Inferring anatomical connectivity using diffusion MR imaging. NeuroImage 37, 474–488.

Kaden, E., Anwander, A., Knösche, T.R., 2008. Variational inference of the fiber orientation density using diffusion MR imaging. NeuroImage 42, 1366–1380.

Klein, A., Andersson, J., Ardekani, B.A., Ashburner, J., Avants, B., Chiang, M.C., Christensen, G.E., Collins, D.L., Gee, J., Hellier, P., Song, J.H., Jenkinson, M., Lepage, C., Rueckert, D., Thompson, P., Vercauteren, T., Woods, R.P., Mann, J.J., Parsey, R.V., 2009. Evaluation of 14 nonlinear deformation algorithms applied to human brain MRI registration. NeuroImage 46, 786–802.

Koch, M.A., Norris, D.G., Hund-Georgiadis, M., 2002. An investigation of functional and anatomical connectivity using magnetic resonance imaging. NeuroImage 16, 241–250.

Kreher, B.W., Mader, I., Kiselev, V.G., 2008. Gibbs tracking: a novel approach for the reconstruction of neuronal pathways. Magn. Reson. Med. 60, 953–963.

Lazar, M., Weinstein, D.M., Tsuruda, J.S., Hasan, K.M., Arfanakis, K., Meyerand, M.E., Badie, B., Rowley, H.A., Haughton, V., Field, A., Alexander, A.L., 2003. White matter tractography using diffusion tensor deflection. Hum. Brain Mapp. 18, 306–321.

Lebel, C., Walker, L., Leemans, A., Phillips, L., Beaulieu, C., 2008. Microstructural maturation of the human brain from childhood to adulthood. NeuroImage 40, 1044–1055.

Leergaard, T.B., White, N.S., de Crespigny, A., Bolstad, I., D'Arceuil, H., Bjaalie, J.G., Dale, A.M., 2010. Quantitative histological validation of diffusion MRI fiber orientation distributions in the rat brain. PLoS One 5, e8595.

Lenglet, C., Campbell, J.S.W., Descoteaux, M., Haro, G., Savadjiev, P., Wassermann, D., Anwander, A., Deriche, R., Pike, G.B., Sapiro, G., Siddiqi, K., Thompson, P.M., 2009. Mathematical methods for diffusion MRI processing. NeuroImage 45, S111–S122.

Leuze, C.W.U., Anwander, A., Bazin, P.-L., Dhital, B., Stüber, C., Reimann, K., Geyer, S., Turner, R., 2014. Layer-specific intracortical connectivityrevealed with diffusion. MRI. Cereb. Cortex 24 (2), 328–339.

Malcolm, J.G., Kubicki, M., Shenton, M.E., Rathi, Y., 2009. The effect of local fiber model on population studies. In Diffusion Modeling and Fiber CupMICCAI, London, UK 33–40.

Melonakos, J., Mohan, V., Niethammer, M., Smith, K., Kubicki, M., Tannenbaum, A., 2007. Finsler Tractography for White Matter Connectivity Analysis of the Cingulum Bundle. Medical Image Computing and Computer-Assisted Intervention—MICCAI 2007. Springer, Berlin Heidelberg 36–43.

Mori, S., van Zijl, P.C.M., 2002. Fiber tracking: principles and strategies — a technical review. NMR Biomed. 15, 468–480.

Mori, S., Oishi, K., Jiang, H., Jiang, L., Li, X., Akhter, K., Hua, K., Faria, A.V., Mahmood, A., Woods, R., Toga, A.W., Pike, G.B., Neto, P.R., Evans, A., Zhang, J., Huang, H., Miller, M.I., van Zijl, P., Mazziotta, J., 2008. Stereotaxic white matter atlas based on diffusion tensor imaging in an ICBM template. NeuroImage 40, 570–582.

Nelder, J.A., Mead, R., 1965. A simplex method for function minimization. Comput. J. 7, 308–313.

Nichols, T.E., Holmes, A.P., 2002. Nonparametric permutation tests for functional neuroimaging: a primer with examples. Hum. Brain Mapp. 15, 1–25.

O'Donnell, L.J., Westin, C.-F., Golby, A.J., 2009. Tract-based morphometry for white matter group analysis. NeuroImage 45, 832–844.

Pichon, E., Westin, C.-F., Tannenbaum, A.R., 2005. A Hamilton–Jacobi–Bellman Approach to High Angular Resolution Diffusion Tractography. Medical Image Computing and Computer-Assisted Intervention—MICCAI 2005. Springer, Berlin Heidelberg 180–187.

Poupon, C., Rieul, B., Kezele, I., Perrin, M., Poupon, F., Mangin, J.F., 2008. New diffusion phantoms dedicated to the study and validation of high-angular-resolution diffusion imaging (HARDI) models. Magn. Reson. Med. 60, 1276–1283.

Raffelt, D., Tournier, J.D., Rose, S., Ridgway, G.R., Henderson, R., Crozier, S., Salvado, O., Connelly, A., 2012. Apparent fibre density: a novel measure for the analysis of diffusion-weighted magnetic resonance images. NeuroImage 59, 3976–3994.

Reisert, M., Mader, I., Kiselev, V., 2009. Tracking a physical phantom by global fibre reconstruction. MICCAI Workshop on Diffusion Modelling and the Fiber Cup, London, United Kingdom. MICCAI, Springer.

Reisert, M., Mader, I., Anastasopoulos, C., Weigel, M., Schnell, S., Kiselev, V., 2011. Global fiber reconstruction becomes practical. NeuroImage 54, 955–962.

Riffert, T., Knösche, T.R., Anwander, A., 2012. Quantification of fiber bundle properties using a decomposition of the fiber orientation distribution function. Proc. Int. Soc. Magn. Reson. Med. 20, 3592 (Melbourne, Australia).

Riffert, T., Schreiber, J., Anwander, A., Knösche, T.R., 2014w. Beyond Fractional Anisotropy: Extraction of Bundle-Specific Structural Metrics from Crossing-Fiber Models (under review).

Ros, C., Güllmar, D., Stenze, M., Mentzel, H.J., Reichenbach, J.R., 2012. Quantitative fiber bundle-based analysis of diffusion-weighted MRI data. Biomed. Tech. (Berl.) 57, 530–533.

Savadjiev, P., Rathi, Y., Bouix, S., Smith, A.R., Schultz, R.T., Verma, R., Westin, C.F., 2013. Combining surface and fiber geometry: an integrated approach to brain morphology. MICCAI 2013. Springer, Berlin Heidelberg, pp. 50–57.

Schultz, T., Seidel, H.P., 2008. Estimating crossing fibers: a tensor decomposition approach. IEEE Trans. Vis. Comput. Graph. 14, 1635–1642.

Smith, S.M., Nichols, T.E., 2009. Threshold-free cluster enhancement: addressing problems of smoothing, threshold dependence and localisation in cluster inference. NeuroImage 44, 83–98.

Smith, S.M., Jenkinson, M., Woolrich, M.W., Beckmann, C.F., Behrens, T.E.J., Johansen-Berg, H., Bannister, P.R., Luca, M.D., Drobnjak, I., Flitney, D.E., Niazy, R.K., Saunders, J., Vickers, J., Zhang, Y., Stefano, N.D., Brady, J.M., Matthews, P.M., 2004. Advances in functional and structural MR image analysis and implementation as FSL. NeuroImage 23 (Suppl. 1), S208–S219.

Smith, S.M., Jenkinson, M., Johansen-Berg, H., Rueckert, D., Nichols, T.E., Mackay, C.E., Watkins, K.E., Ciccarelli, O., Cader, M.Z., Matthews, P.M., Behrens, T.E.J., 2006. Tract-based spatial statistics: voxelwise analysis of multi-subject diffusion data. NeuroImage 31, 1487–1505.

Smith, R.E., Tournier, J.-D., Calamante, F., Connelly, A., 2013. SIFT: spherical-deconvolution informed filtering of tractograms. NeuroImage 67, 298–312.

Snook, L., Plewes, C., Beaulieu, C., 2007. Voxel based versus region of interest analysis in diffusion tensor imaging of neurodevelopment. NeuroImage 34, 243–252.

Song, S.-K., Sun, S.-W., Ramsbottom, M.J., Chang, C., Russell, J., Cross, A.H., 2002. Dysmyelination revealed through MRI as increased radial (but unchanged axial) diffusion of water. NeuroImage 17, 1429–1436.

Sotiropoulos, S.N., Behrens, T.E., Jbabdi, S., 2012. Ball and rackets: inferring fiber fanning from diffusion-weighted MRI. NeuroImage 60 (2), 1412–1425.

Tournier, J.D., Calamante, F., Gadian, D.G., Connelly, A., 2004. Direct estimation of the fiber orientation density function from diffusion-weighted MRI data using spherical deconvolution. NeuroImage 23, 1176–1185.

Tournier, J.D., Calamante, F., Connelly, A., 2007. Robust determination of the fibre orientation distribution in diffusion MRI: non-negativity constrained super-resolved spherical deconvolution. NeuroImage 35, 1459–1472.

Tournier, J.D., Calamante, F., Connelly, A., 2012. MRtrix: diffusion tractography in crossing fiber regions. Int. J. Imaging Syst. Technol. 22, 53–66.

Tuch, D., 2002. Diffusion MRI of Complex Tissue Structure. (PhD Thesis) Harvard University and Massachusetts Institute of Technology, Boston, USA.

Tuch, D.S., 2004. Q-ball imaging. Magn. Reson. Med. 52, 1358–1372.

Tuch, D.S., Reese, T.G., Wiegell, M.R., Makris, N., Belliveau, J.W., Wedeen, V.J., 2002. High angular resolution diffusion imaging reveals intravoxel white matter fiber heterogeneity. Magn. Reson. Med. 48, 577–582.

Turken, A.U., Dronkers, N.F., 2011. The neural architecture of the language comprehension network: converging evidence from lesion and connectivity analyses. Front. Syst. Neurosci. 5.

Wedeen, V.J., Reese, T.G., Tuch, D.S., Dou, J.G., Weiskoff, R.M., Chessler, D., 2000. Mapping fiber orientation spectra in cerebral white matter with Fourier-transform diffusion MRI. Proc. Int. Soc. Magn. Reson. Med. 321 (Denver, USA).

Woolrich, M.W., Jbabdi, S., Patenaude, B., Chappell, M., Makni, S., Behrens, T., Beckmann, C., Jenkinson, M., Smith, S.M., 2009. Bayesian analysis of neuroimaging data in FSL. NeuroImage 45, S173–S186.

Yo, T.-S., Anwander, A., Descoteaux, M., Fillard, P., Poupon, C., Knösche, T., 2009. Quantifying brain connectivity: a comparative tractography study. Proc Med Image Comput Comput Assist Interv, vol. 1. MICCAI, London, UK 886–893.

Yushkevich, P.A., Zhang, H., Simon, T.J., Gee, J.C., 2008. Structure-specific statistical mapping of white matter tracts. NeuroImage 41, 448–461.

Zhang, H., Hubbard, P.L., Parker, G.J.M., Alexander, D.C., 2011a. Axon diameter mapping in the presence of orientation dispersion with diffusion MRI. NeuroImage 56, 1301–1315.

Zhang, H., Dyrby, T.B., Alexander, D.C., 2011b. Axon diameter mapping in crossing fibers with diffusion MRI. Proc Med Image Comput Comput Assist Interv, vol. 2. MICCAI, Toronto, Canada 82–89.

Zhang, H., Schneider, T., Wheeler-Kingshott, C.A., Alexander, D.C., 2012. NODDI: practical in vivo neurite orientation dispersion and density imaging of the human brain. NeuroImage 61 (4), 1000–1016.